Molecular Dynamics Simulation of Amphiphilic Aggregates

By
Lanyuan Lu

A dissertation submitted to the faculty of the University of North Carolina at Chapel Hill in partial fulfillment of the requirements for the degree of Doctor of Philosophy in the Department of Chemistry.

Chapel Hill
2006

Approved by,

Max L. Berkowitz, Advisor

John M. Papanikolas, Reader

Garegin A. Papoian, Reader

ABSTRACT

Lanyuan Lu: Molecular Dynamics Simulation of Amphiphilic Aggregates
(Under the Direction of Max L. Berkowitz)

In this dissertation, molecular dynamics simulations were performed for systems containing amphiphilic aggregates, such as monolayers, bilayers, and reverse micelles. Various analysis methods were used in order to investigate structural and dynamical properties and solve particular problems for different systems.

First, we present simulations where we observed successful self-assembly of reverse micelles in a three-component system containing supercritical CO_2, water, and fluorinated surfactant starting from random configurations. Such self-assembly allows for the future computational study of structural and thermodynamic properties of microemulsions in water/CO_2 systems that will be less dependent on the initial conditions.

Next, a series of molecular dynamics simulations were performed to study the PFPE (perfluoropolyether) and PE (polyether) surfactant monolayers and micelles at the water/supercritical carbon dioxide interface. We observed that values of intramolecular bonded interaction parameters which are related to chain rigidity determine the monolayer surface pressure. We show that "good" and "bad" properties of PFPE/PE surfactants are connected to conformational entropy.

In order to study the effect of the hydration force, we simulated systems with model hydrophilic plates. We studied the effect of charge correlation on the potential of mean force between plates. The orientational structure of water between the plates was investigated to

understand the effect of molecular structure of water on the properties of the potential of mean force.

Finally, we calculated the free energy cost for removing a cholesterol molecule from two different lipid bilayers. The results can help us to understand the relationship between the lipid structure and the lipid-cholesterol affinity. N-palmitoyl-sphingomyelin was found to have a better cholesterol affinity compared with that of phosphatidylcholine lipid DPPC, according to our free energy values from molecular dynamics simulations.

ACKNOWLEDGMENTS

I would like to thank, first of all, my advisor, Professor Max L. Berkowitz for his careful guidance. He is always very patient when I need help in my research. I learned a lot from his insight and serious-minded attitude in the academic work. He teaches me not only the knowledge in science, but also the way to be a successful person.

I would also like to thank Professor Joseph M. DeSimone, John M. Papanikolas, Garegin A. Papoian, and H. Holden Thorp in my doctoral committee for their precious time and encouragement.

There are many people who have helped me for my research work. I thank former postdocs in my group: Dr. Sanjib Senapati, Dr. Sargar Pandit, Dr. Luis G. Dias, and Dr. Shreyas Behide. I also thank former student Dr. David L. Bostick. It is hard to imagine that I can finish my Ph.D research without the warm-hearted help from above people and numerous stimulating discussions. I would thank Charles Davis for checking grammars for part of this dissertation.

Finally, I would thank my parents in China, for their continuous support during my five and half years of graduate study.

CONTENTS

LIST OF TABLES

LIST OF FIGURES

Chapter 1

Introduction

The term amphiphile usually refers to a molecule that contains both hydrophobic and hydrophilic parts. A large variety of molecules are amphiphiles, including surfactants and lipids, some polymers and proteins. In a typical amphiphilic molecule, the hydrophilic part is often called “headgroup”. The headgroup can be a charged moiety such as $–PO_4^-$ in many phosphate surfactants, or a zwitterionic neutral group such as phosphatidylcholine headgroup in PC lipids. Surfactants always have a “tail” as their hydrophobic part. The main component of the hydrophobic tail usually consists of alkane chains or other hydrophobic structure with a small dipole moment.

Due to the favorable dipole-dipole headgroup-water interaction and relatively unfavorable water-tail interaction, amphiphilic molecules want to adjust their conformations and aggregate in order to minimize the contacts between water phase and hydrophobic tails. If hydrophobic oil solvent is present besides water solvent, the amphiphile will also want to maximize the tail-oil contact. As a result, the amphiphilic molecules display different aggregation morphologies including monolayers, bilayers, micelles, reverse micelles, vesicles, etc. A large amount of experimental and theoretical study has been performed on

these amphiphile aggregates due to their important role in many physical and biological processes.

The Molecular dynamics (MD) simulation technique is a powerful tool to study amphiphile aggregates. In a MD simulation, we can obtain structures of aggregates and conformations of amphiphilic molecules by using appropriate force fields and equations of Newton's laws of motion. Molecular interaction energy and the free energy profiles can be also calculated from simulation data. This provides us with a detailed microscopic view of the system we want to study and with information that is very hard to obtain directly from experiments. The theoretical study of the relationship between molecular interactions and aggregate properties can help us to understand fundamental physical principles behind many phenomena in biophysics and surface science. Another important application of MD simulations in this field is in helping to design new amphiphiles in order to obtain required aggregate properties. Since MD simulations can also provide information on dynamics, one can study amphiphile self-assembly and other dynamical processes.

In this dissertation, we will present our simulations on various amphiphile aggregates, including surfactant monolayers, surfactant reverse micelles and lipid bilayers. The first half of this dissertation deals with systems containing surfactants. This includes surfactant micellar self-assembly and properties of surfactant micelles and monolayers. The second part deals with lipid bilayers. In all the described work, MD simulations, along with many different analysis methods including free energy calculations, have been used in order to study the relationship between microscopic interactions and the macroscopic properties of aggregates.

In chapter 2, we present an investigation of surfactant self-assembly. This is an

interesting example demonstrating how the increase in computational power helped in solving a special problem that was computationally forbidden for old generation computers. Because the simulation of self-assembly may avoid creation of the meta-stable states which result from the artificial initial conformation, it is desirable to perform such simulations to obtain more convincing equilibrated structures.

Chapter 3 presents a simulation study of surfactant monolayers at the water/carbon dioxide environment. Through this particular case, we show how structure-function relationships can be studied using MD simulations. In MD simulations, we model the systems of our concern with force fields, usually on atomistic level. Various force field parameters are systematically changed in our study in order to reveal the structure based mechanism for high surface activity. In MD simulations we can directly observe the microscopic structure of surfactants. Thus some ideas in surfactant design related to notions such as excluded volume and surfactant rigidity can be checked using simulation data. The energy-entropy decomposition can also be performed by analyzing MD trajectories. Thus we can link the surfactant structure to thermodynamic quantities such as surface tension. Conclusions from our simulation studies may help in establishing theoretical principles of surfactant design.

Sometimes, due to the complexity of the system that we want to study, a simplified model is preferred in order to remove minor effects while maintaining the basic physical picture. In Chapter 4, we consider such a case, when we study the hydration forces acting between lipid membranes. Hydration repulsive forces acting between hydrophilic surfaces such as lipid bilayers have been observed in many experimental studies, especially the ones performed using the atomic force microscopy (AFM) method [87]. Although there are many

experimental and theoretical papers [87] in literature trying to explain unusual repulsive forces, the physics behind it is still under debate. Because there are many different interactions between the hydrophilic surfaces, it is quite difficult to pick out the main effect from the simulation data using the full atomistic model. Another reason to simplify the model is the concern of computational efficiency. By simulating a simple model system we can obtain more data for force-distance relation. Thus a semi-quantitative comparison to theoretical predictions can be achieved. In most theoretical works, the hydration force is a result of the electrostatic interaction between surfaces and water solvent. Hence, we simulate hydrophilic surfaces as Lennard-Jones plates decorated with dipoles and calculate the interaction free energy between these plates. By changing arrangements of dipoles on the surfaces, we obtain different types of interaction between plates. Our simulation results can help us to understand the nature of hydration forces alone.

The last chapter of this dissertation presents a study of the interaction between cholesterol molecule and lipid bilayer. In this study, we calculated the potential of mean force (PMF) of removing one cholesterol molecule from various lipid bilayers in order to understand the cholesterol-bilayer interaction. In many cases, we are more interested in system free energy instead of energy which can be calculated directly from MD trajectories. The term PMF refers to the free energy as a function of some particular order parameter (in our case, the distance between the center of mass of cholesterol and the center of the bilayer). In order to obtain PMF, a series of MD simulations with biased potential needs to be performed and the PMF can be calculated using umbrella sampling technique [41, 72]. In chapter 5, the affinity between lipid bilayer and cholesterol can be quantitatively obtained from our PMF data. This affinity is helpful in understanding biological processes such as

membrane raft formation [8]. By comparing cholesterol affinity for different lipid bilayers, we can understand the relationship between lipid structure and cholesterol-bilayer interaction.

Chapter 2

Molecular Dynamics Simulation of a Reverse Micelle Self-assembly in Supercritical CO_2

2.1 MD Simulation of Self-assembly

In principle, the result of an MD simulation is not dependent on the starting conformation of the simulated system. During a simulation, the conformational space is explored and the system finally goes to equilibrium. If there is a unique conformation corresponding to the global free energy minimum, we usually expect that we can observe equilibrated conformations in our MD simulation most often near this particular minimum. However, the initial conformation still needs to be chosen with care for most systems due to two major reasons. The first concern is the computer time needed to reach the equilibrium.

All-atom simulations are usually time-consuming, especially for large systems. As a result, an initial conformation near the equilibrium is always preferred in order to reduce the total simulation time. The second reason is related to the existence of the meta-stable states in which the system can be trapped. Usually there are a few meta-stable states on the free energy surface of a simulated system. Once a system goes to one of these states, it takes a long time for it to come out. The most efficient way to avoid these meta-stable states is of course to start with the initial state near the equilibrium.

Based on the discussion above, the initial structures in most MD simulations are usually taken from experimental data or theoretical prediction. For instance, in micellar simulations, a pre-assembled micelle is the standard initial conformation for MD. Contrary to that, in self-assembly simulations the molecules are arranged in a random and scattered distribution. The target aggregated conformation such as a micelle can be formed during the MD simulation without any external influence. In general, the self-assembly of a micelle should be preferred in computational studies, since less dependence on the initial conditions (and number of particles) is expected to appear in the simulation.

Computer simulation of self-assembly is a challenge for computational studies [69]. With the increasing power of modern computers, it is now possible to study various self-assembly processes in atomic detail using MD simulations. In recent years, Marrink and co-workers observed the spontaneous aggregation of direct micelles [57], bilayers [16], and vesicles [56]. In these simulations the typical time scale of self-assembly was ~10-100 ns or even longer.

Reverse Micelle (RM) is another ideal system for performing self-assembly MD simulations. Unlike previously mentioned two-component systems, there are three different

components in a RM system. For a water-in-oil RM, the inner aqueous core usually consists of water and counter ions. There are amphiphilic molecules (usually surfactants) surrounding the aqueous core with headgoups pointing to inner side direction. We obtain a RM by combining the above two components together. Oil phase is outside of the RM forming a water-surfactant-oil system. In nature there are also oil-in-water RMs with similar buildup. The self-assembly of such a RM has never been simulated satisfactorily before our work, although has been attempted [74, 75].

2.2 Models and Methods

In our molecular dynamics simulations the $scCO_2$/surfactant/water system was chosen to study self-aggregation behavior. Here $scCO_2$ means supercritical carbon dioxide which acts as oil solvent phase. We used the fluorinated polyether, CF_3-(O-CF_2-$CF(CF_3)$)$_3$-O-CF_2-COO^- NH_4^+ (PFPE), M_w=695.13, as the surfactant, which is a commercially available surfactant found to form aqueous reverse micelles in $scCO_2$. Experiments show [35, 95] that PFPE forms aqueous RMs in scCO2 with water-surfactant mole ratios (W_0) up to 30. We also performed simulations with the hydrogenated analogue of the PFPE surfactant, PE.

In the simulations, the force field for the anionic surfactants and water were the same as those used by Senapati and Berkowitz [78]. The consistent valence force field [15] (CVFF) was used to describe the surfactant anions. Accelrys's Material Studio software was used to calculate the point charges [1]. The OPLS set of intermolecular parameters was used to

describe the NH_4^+ counterions [36] and a well-known SPC/E model was used to describe water molecules [3]. The detailed discussion of surfactant force field parameters can be also found in next chapter when we are discussing the relation between force field parameters and surface activity. In this chapter we will focus on self-assembly behavior. For reason of computational economy, a single-point model was used for the CO_2 molecules [29]. We demonstrated previously [79] that this model gives a good description of the $scCO_2$ equation of state. In our primary simulation, there are 66 PFPE molecules, 554 water molecules and 6359 CO_2 molecules. The temperature (298 K) and the pressure (20 MPa) in the ensemble (NPT) we used here were also the same as in the above mentioned work of Senapati and Berkowitz [78]. All simulations were performed using molecular dynamics software package GROMACS [4, 47].

To understand the factors that determine micelle formation, a series of simulations was performed. In two of the simulations, the simulation box contained 554 water molecules, 66 fluorinated surfactant molecules (W_0=8.4), and 6359 CO_2 molecules. These numbers of particles are exactly the same as in the simulation of Senapati and Berkowitz [78]. In the first simulation the molecules were initially distributed randomly, and in the second, the initial positions were distributed on a regular lattice. Each simulation lasted for more than 50 ns to ensure thermodynamic equilibrium. We also investigated the effect of different W_0's on the process of the micellar formation. This is achieved by changing of molecule numbers in the simulation box.

2.3 Results and Discussions

2.3.1 Self-assembly of a Reverse Micelle in CO_2

In our total simulation time of 50 ns for each different initial condition, the self-assembly process was observed can be divided into several stages. In the first stage water and surfactant molecules rearranged themselves and clustered into several small micelle-like aggregates. This process typically took around 1 ns in our MD simulation. The fast first stage was followed by a slower process during which three or four small micelles merged into two. The final rearrangement of the last two micelles into one spherical RM was the most time-consuming process.

Various analyses were performed for the self-assembly of PFPE system with random initial conformation. Snap shots taken form MD output trajectory for this system has been show in Figure 2.1. In order to analyze the fast to slow self-assembly behavior, we plotted the number of aggregates as a function of time for this FPPE case as shown in Figure 2.2. In this work, aggregates number N is calculated based on an efficient cluster-counting algorithm proposed by Sevick et al [80]. From Figure 2.2 the number of cluster shows an exponential like decay from around 70 to one when simulation time is increasing. The system evolved into a single micelle at a time point after 4 ns. This result is consistent with our observation from snap shots and is similar to the dynamics observed by Marrink et al [57]. Average water inter-molecular distance was also plotted in order to study the self-assembly dynamics. As we can see in Figure 2.3 the water inter-molecular distance also shows an exponential like decay

and it reaches a stable value after 4 ns. Thus from above analyses the fast to slow self-assembly behavior can be confirmed. For this PFPE system, around 50ns simulation time is needed for the system to reach equilibrium.

Similar analyses have been performed on the PFPE system with lattice initial conformation. The dynamics of self-assembly was found to be close to previous results for system with random initial conformation. This shows that our self-assembly process is not sensitive on the choice of initial scattered conformation. The self-assembly dynamics of PE counterpart is also similar while the final aggregate structure is dramatic different.

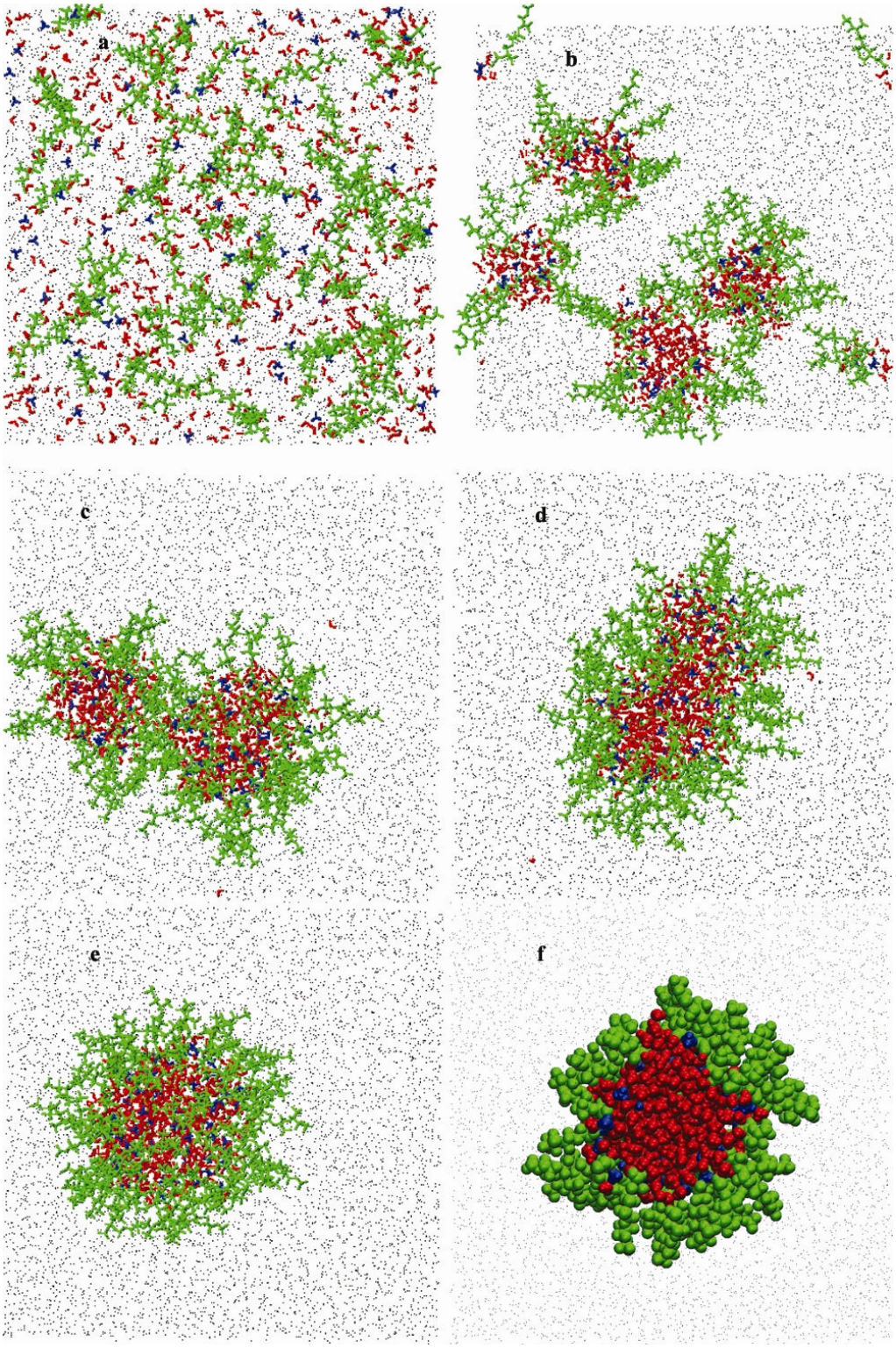

Figure 2.1: Snapshots of the PFPE RM self-assembly (554 water and 66 surfactant molecules). Red, blue, and green particles are water, ammoniumions, and PFPE anions, respectively. Small black dots are carbon dioxide molecules. The snapshots are taken at (a) 0 ns; (b) 1 ns; (c) 4 ns; (d) 4.4ns; (e) 5 ns; (f) 50 ns; This snapshot in (f) is of a cut across the micelle to show water in the core and surfactants at the surface.

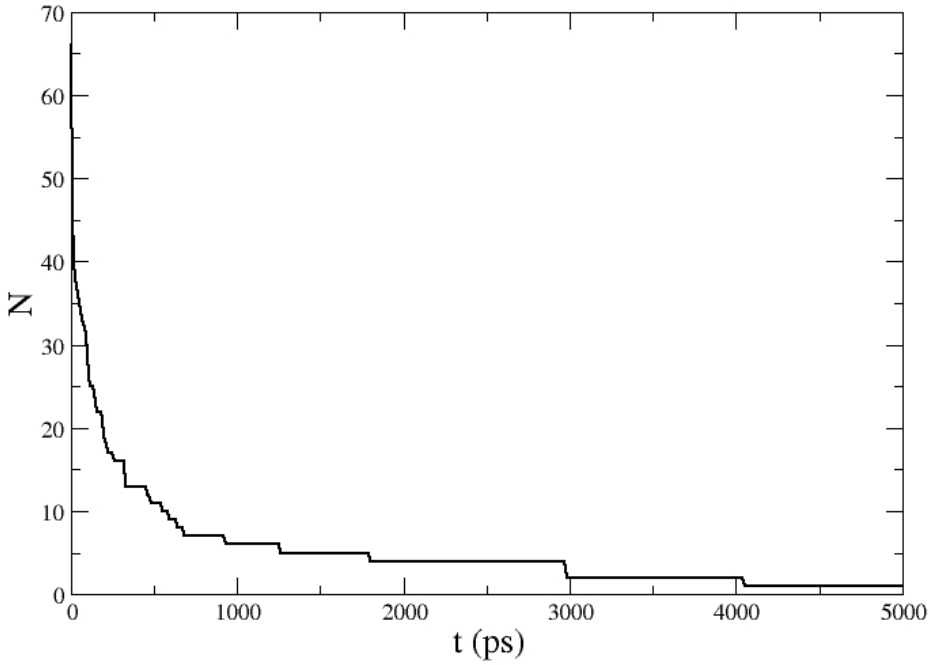

Figure 2.2: Number of aggregates in the PPFE system with random initial conformation as a function of simulation time.

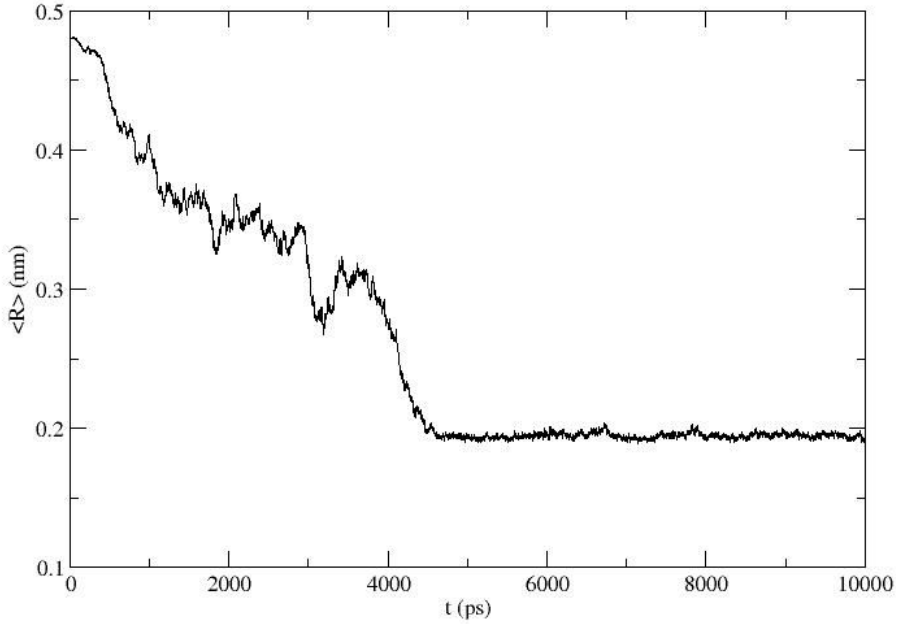

Figure 2.3: The average distance between water molecules in the system with random initial conformation.

2.3.2 Micellar Structure

PFPE micellar structure

We first calculated various properties of the PFPE micelle after self-assembly. In order to measure the size of the micelle, its radius of gyration, R_g was calculated. Here R_g was calculated for the aqueous core of the micelle, by using the following definition:

$$R_g^2 = \sum_i m_i (r_i - r_0)^2 / \sum_i m_i \qquad (2.1)$$

In the equation above i includes water molecules in the core, NH_4^+ counterions, the carboxylate group, the adjacent CF_2 group, and the first ether oxygen in each of the surfactant tails. All these atoms make up the whole aqueous core. This definition of the aqueous core is based on choosing atoms that have close contacts with inner-core water molecules, same as the definition used by Senapati and Berkowitz [78]. The m_i in the same equation refers to the mass of each atom and the r_i-r_0 is the distance for each atom from the center of mass position r_0. For a spherical object with uniform density distribution, its radius R_c can be simply determined by this relation $R_c^2=(3/5)R_g^2$. The same relation is used in light scattering experiments in order to measure micellar radius. In Figure 2.4 the R_c obtained from the last 5ns of our simulation was plotted. The relatively small fluctuation of the data shows that our micelle conformation is stable. The average R_c is 19.1±0.2 Å, which is very close to the result from Senapati and Berkowitz [78]. This result is in good agreement with the experimental value of 20 Å [61], and both numbers from pre-assembled simulation and self-assembly simulation are reasonable.

Average area per headgroup A_h can be easily calculated based on the value of the

micellar radius. If we assume that the aqueous core is spherical, we have

$$A_c = 4\pi R_c^2 = A_h N_h \tag{2.2}$$

where A_c is the total surface area of the aqueous core, and N_h is the total number of surfactant molecules. Thus we obtain the value of A_h as 69.5 $Å^2$, which is in reasonable agreement with the experimental value 76 $Å^2$ [61].

In order to show that our micelle is indeed spherical, we calculated its eccentricity. This provides us with a quantitative measure of the micellar shape. The definition of eccentricity is

$$e = 1 - \frac{I_{\min}}{I_{avg}} \tag{2.3}$$

where I_{min} is the smallest moment of inertia of the micelle along the x, y, or z axis and I_{avg} is the average of all three moments of inertia. All micellar atoms including water, counterions and surfactants were counted in the calculation of moments of inertia. The time evolution of eccentricity is plotted in Figure 2.5. Here we observe that the eccentricity value is close to zero with small fluctuations. The average e is 0.04±0.02 in our PFPE case. For a perfect sphere, eccentricity should be zero. Hence our micelle from self-assembly is indeed like a sphere because of the small value of eccentricity. This confirms our observation from the snapshots of MD trajectories.

We also investigated the effect of different W_0's on the process of the micellar formation. Thus, we performed three more simulations on systems containing (a) 66 surfactant and 1108 water molecules, (b) 66 surfactant and 270 water molecules, and (c) 66 surfactant and 139 water molecules. In all cases we also observed self-assembly, and in cases (a) and (b) the micellar shape was spherical. In case (c) the micelle had a wormlike shape. Although in case (a) the micelle remained spherical and the surfactants were uniformly

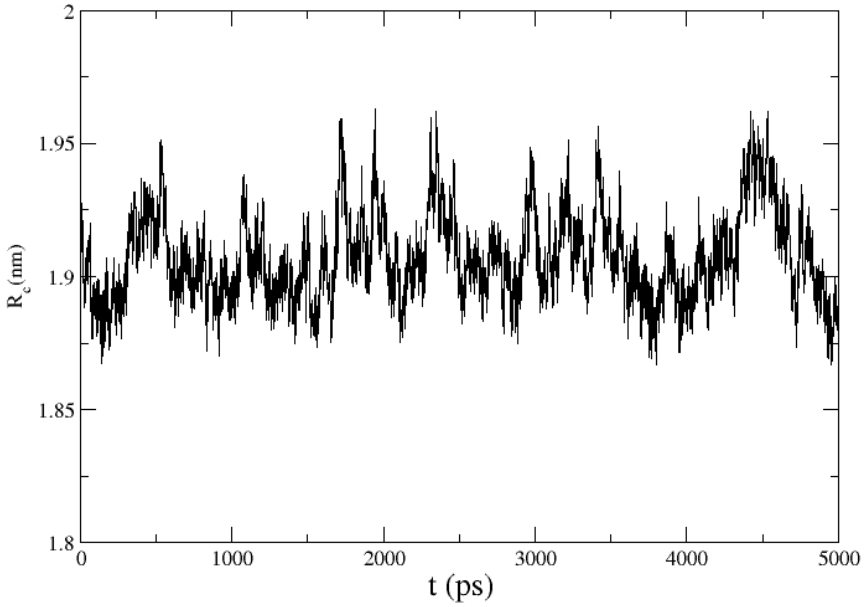

Figure 2.4: Core radius as a function of time in the last 5 ns for the primary PFPE system.

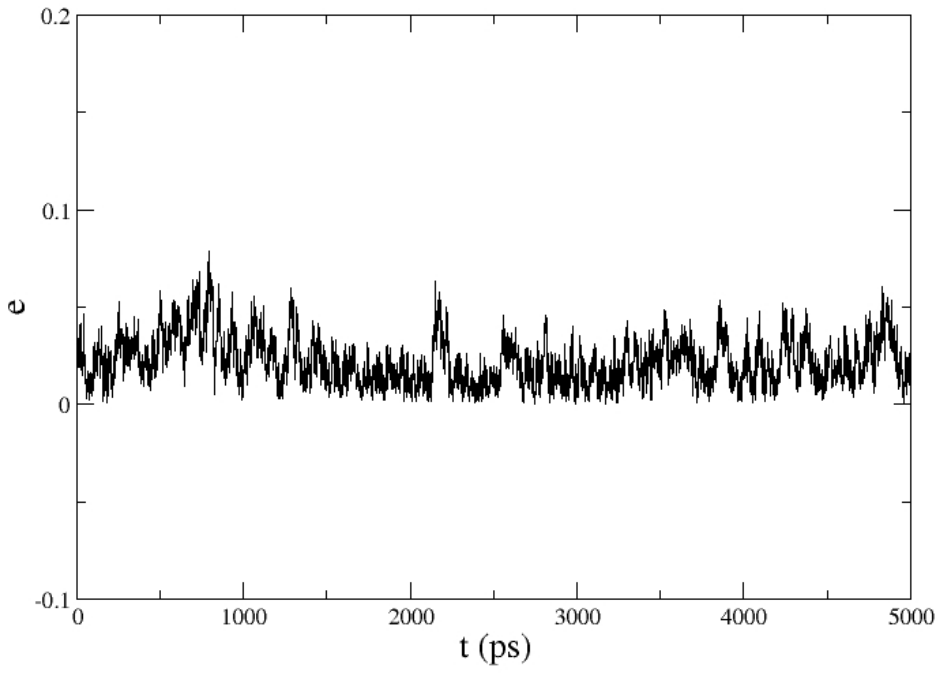

Figure 2.5: Eccentricity as a function of time in the last 5 ns for the primary PFPE system

distributed over the surface of the sphere, we observed a larger contact between water and $scCO_2$ due to a large surface area of the water core.

PE aggregate structure

In the simulation containing 66 PE surfactants and 554 water molecules, we observed self-assembly into a micellar-type aggregeate but with one side of this aggregate having a direct water/$scCO_2$ contact (See Figure 2.6). Such a contact increases the surface tension and, therefore, the free energy of the micelle, indicating that in our system the PE surfactant is not effective for creation of a microemulsion.

To see if we could create a RM containing a uniform distribution of PE surfactants, we decreased the number of water molecules in a few other simulations with PE. In each of these cases we observed aggregates containing regions of direct contact between water and CO_2, like those observed in Figure 2.6. When the number of water molecules became small, the aggregate had a wormlike shape.

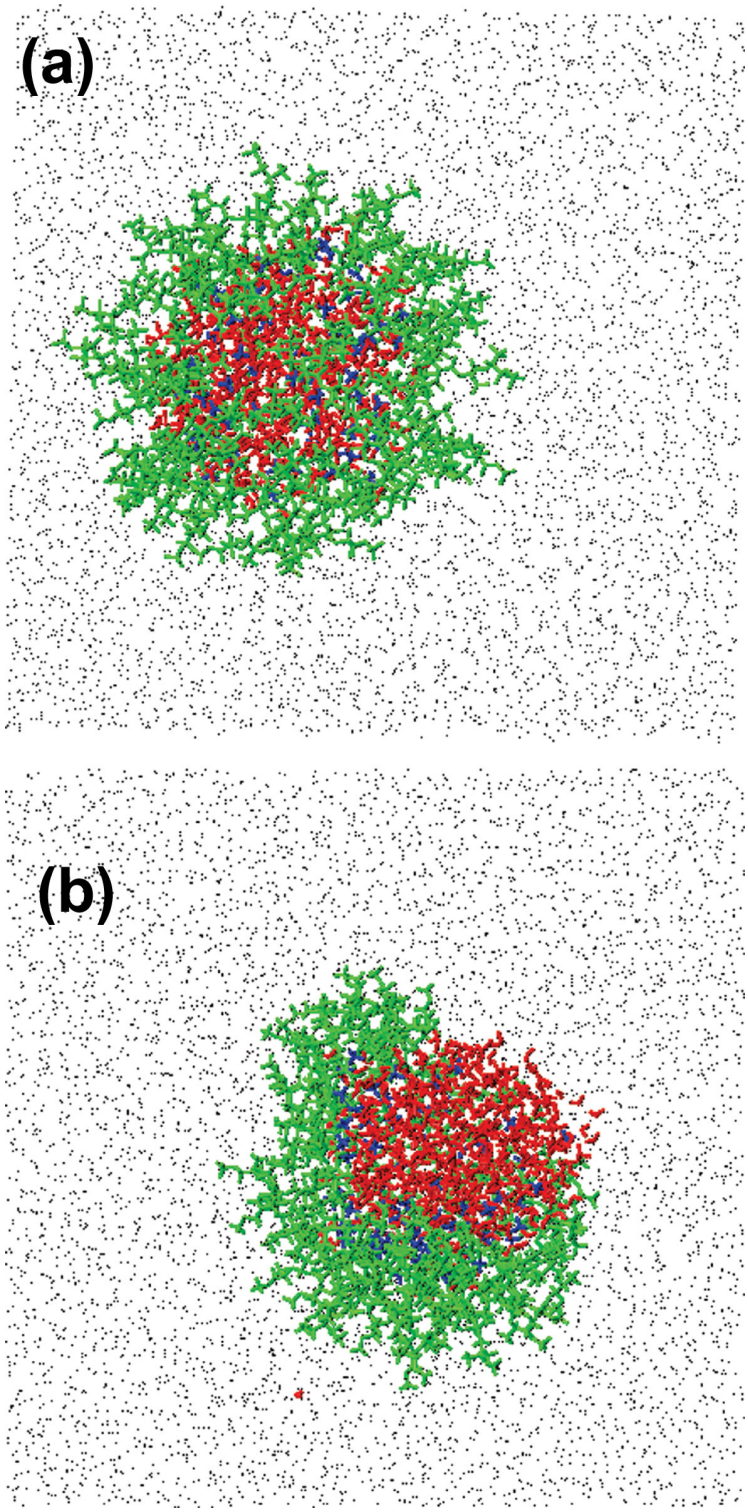

Figure 2.6: Structures of (a) PFPE and (b) PE aggregates from self-assembly. Each structure is after 50 ns of MD simulation. The meaning of colors is the same as that in Figure 2.1.

2.4 Conclusions

In summary, we showed for the first time that, simulating a system containing three components such as water, $scCO_2$, and polyether surfactants on a relatively detailed atomic level, one can observe a self-assembly of molecules after relatively short periods of time. Various micellar physical properties was calculated and compared with results from previous pre-assembled simulations [78]. No obvious difference was observed between the two sets of structures. This consistency validates the pre-assembled simulation in literature. The previous simulation was not trapped in any meta-stable structure. If, in general, RMs are quickly assembled in computer simulations, then, with detailed descriptions of molecules, one can study these micelles in detail in their most stable states.

When the surfactant is fluorinated (PFPE), the self-assembled aggregate represents a nicely shaped RM. In this case stable RMs are observed for a wide range of W_0. When a hydrogenated analogue of the PFPE surfactant is used, an aggregate represents a micellar-like assembly with a nonuniform distribution of surfactant molecules, thus creating a large contact area between water and CO_2, indicating that the hydrogenated analogue of PFPE is not a good agent for creating microemulsions in w/c systems.

Chapter 3

Behaviors of Perfluoropolyether Surfactant and Its hydrogenated Analog at the Water/Supercritical Carbon Dioxide Interface

3.1 Introduction

Supercritical carbon dioxide ($scCO_2$) is a potentially excellent "green" solvent due to its nontoxicity, recyclability, and tuneability. Unfortunately, many solutes do not dissolve in $scCO_2$. To deal with this obstacle, one can create water in CO_2 (w/c) microemulsions to promote the solubility of solutes. Thus, a need exists in finding surfactant molecules that will

facilitate creation of reverse micelles in pure $scCO_2$. Recently, substantial progress in this direction was accomplished through the use or design of a number of fluorinated or partially fluorinated surfactants [20]. In their turn, fluorinated surfactants are environmentally unfriendly and therefore cannot be utilized in high quantities. Nevertheless, we should study these surfactants to understand what makes them act as "good" surfactants in $scCO_2$ and design environmentally friendly "good" surfactants by imitating properties of fluorinated surfactants and their behavior in $scCO_2$. The main issue related to special properties of fluorinated surfactants in $scCO_2$ is still not understood. Initially, the belief was that specific interactions between fluorinated tails of the surfactant molecules and CO_2 solvent were responsible for the "good" behavior of surfactants, but the ab initio calculations [18] and experiments [93] indicated that such specific interactions do not exist and that the strength of the tail solvent interactions was the same for hydrogenated and fluorinated surfactants.

Stone et al. [83] proposed that the fractional free volume (FFV) available to CO_2 molecules in the tail region can serve as an index for the activity of the surfactant at the water/$scCO_2$ interface. According to Stone et al. the necessary condition for the surfactant to be able to create w/c microemulsion is to have a low FFV. Indeed, most of the examples discussed by Stone et al. demonstrate the usefulness of the FFV concept. Nevertheless, use of only FFV criteria for the determination of the ability to create microemulsions may be incomplete. For example, consider one of the popular fluorinated surfactants: perfluorinated polyether ammonium carboxylate surfactant ($PFPECOO^-NH_4^+$, MW= 695.13). It has a relatively high FFV equal to 0.59, but it is a "good" surfactant, while a "bad" surfactant DiH8, which is a hydrogenated analogue of a fluorinated surfactant DiF8 , has a very similar FFV equal to 0.61 [83]. Micelles with PFPE and its hydrogenated analogue PE were the

subject of previous simulations performed in our group [48, 78]. In the first set of simulations [78] we preassembled the micelles and studied their properties. We observed that the presence of PFPE surfactant generated a nice reverse micelle in CO_2 with water molecules located in a water pool in the micellar interior. The direct contact between water and CO_2 in the reverse micelle was observed to be very small. In the simulations with the PE surfactants, a clustering of PE molecules was observed, and "patches" of a direct water/CO_2 contact appeared. In another set of simulations [48] the micelles were not preassembled, but were self-assembled, thus avoiding creation of artifacts due to the preassembly procedure. The results from our self-assembled and preassembled simulations were very similar and reached the same conclusion: "patches" of direct water/CO_2 contact on micellar surfaces created in the presence of PE surfactants raised the interface tension, which was responsible for the "bad" behavior of the PE surfactant.

In order to find the fundamental difference between PPFE and PE surfactants in microemulsion formation, we first did systematical simulations with micellar geometry. It is hard to calculate and study the surface tension in micellar systems due to the presence of a pronounced interface curvature in these cases. Therefore we decided to learn about the surface properties of PFPE versus PE by performing monolayer simulations for which surface tension can be easily calculated. The results of this study are described below.

3.2 Simulation Details

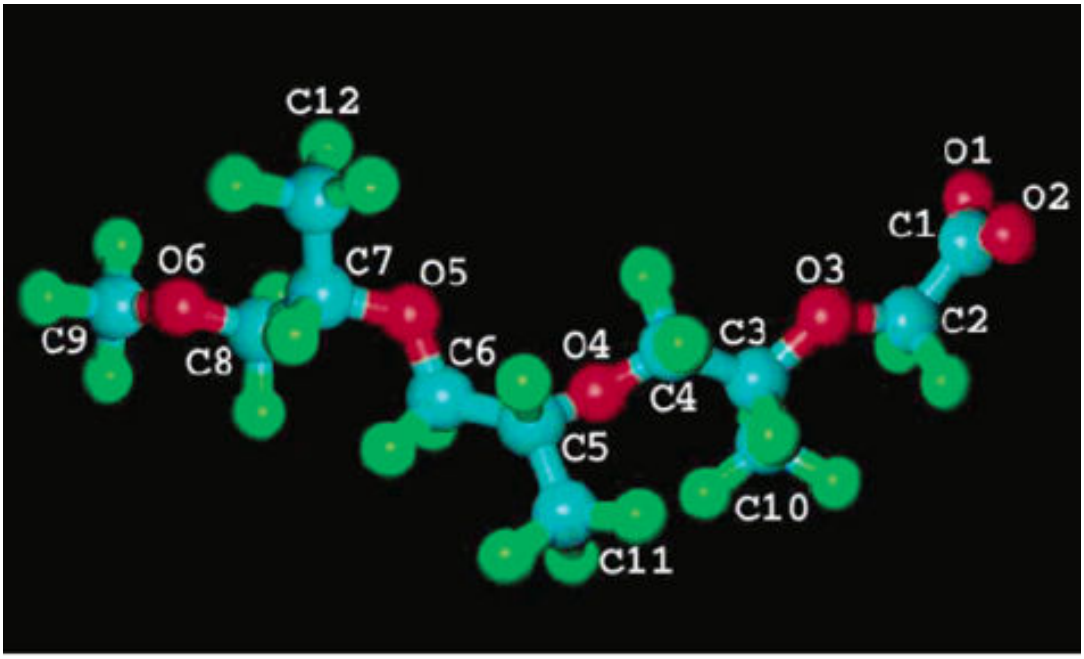

Figure 3.1: Structure of PFPE surfactant anion. Red balls are oxygen atoms; cyan balls are carbon atoms and greed balls are fluorine atoms.

We performed a number of molecular dynamics simulations to understand the difference between PFPE and PE surfactants. The simulations were done on systems containing surfactant micelles and monolayers at the $H_2O/scCO_2$ interface. As in our previous simulations, we used here the consistent valence force field (CVFF) parameters to describe the surfactant anions [15]. Accelrys's Material Studio software was used to calculate the point charges [1]. In Figure 3.1 we show the surfactant structure and atom index numbers which will be used in future discussions. The OPLS set of intermolecular parameters was used to describe the NH_4^+ counterions [36] and a well-known SPC/E model was used to describe water molecules [3]. The parameters for the force field we used in our simulations to describe surfactant anions, counterions, and water can be found in Table 3.1, which were also used in the work of Senapati and Berkowitz [78]. For computational economy a simple

Lennard-Jones model was used to describe CO_2 molecules [29]. Gomes et al. [25] calculated the chemical potential of CO_2 in bulk fluorocarbons and hydrocarbons. They found that the partial charges on CO_2 described by the EPM2 model [27] played only a minor role in determining the value of the chemical potential. This fact somewhat justifies our usage of a single site uncharged sphere for CO_2 molecules in our simulations. More justification follows from the observation that in the previous simulations on reverse micelles containing either PE or PFPE surfactants performed in our group [48, 78], the structural results were similar when the model for CO_2 was the three-site EPM2 model [78] and when it was a single-site Lennard-Jones sphere [48]. We also performed one PFPE self-assembly simulation as the primary simulation in ref[48] and no obvious difference was found for the final micellar structure.

The total potential energy of the system is:

$$U = U_{inter} + U_{intra} \tag{3.1}$$

where U_{inter} and U_{intra} are intermolecular and intramolecular potential energies respectively. The intermolecular potential energy is a sum of short range Lennard -Jones potential and long range Coulomb interaction, as below:

$$U_{inter} = \sum_i \sum_{j>i} 4\varepsilon_{ij}[(\sigma_{ij}/r_{ij})^{12} - (\sigma_{ij}/r_{ij})^{6}] + q_i q_j / r_{ij} \tag{3.2}$$

Here we used Lorentz-Berthelot combining rule for cross terms in LJ interaction

$$\sigma_{ij} = (\sigma_i + \sigma_j)/2 \text{ and } \varepsilon_{ij} = \sqrt{\varepsilon_i \varepsilon_j} \tag{3.3}$$

The intramolecular potential for the surfactant anions has the form:

$$U_{intra;anion} = \sum_i k_{b,i}(r_i - r_0)^2 + \sum_i k_{\theta,i}(\theta_i - \theta_0)^2 + \sum_i A_i[1 + \cos(m\phi_i - \phi_0)] + \sum_i B_i[1 + \cos(n\chi_i - \chi_0)] \tag{3.4}$$

where the four terms on the right hand side represent harmonic bond stretching potential,

Table 3.1: Force field parameters for the various species present in the systems Partial Charges[a].

Atom type	Charge (e)	Atom type	Charge (e)	Atom type	Charge (e)
For H_2O, CO_2 and NH_4^+ Cation					
O_w	-0.8476	C_c	0.6512	N_a	-0.4000
H_w	0.4238	O_c	-0.3256	H_a	0.3500
For $PFPECOO^-$ Anion					
O1,O2	-0.570	O3,O4,O5,O6	-0.300	C9	0.975
C1	0.140	C3,C5,C7	0.425	C10,C11,C12	0.825
C2	0.700	C4,C6,C8	0.700	F	-0.275
For $PECOO^-$ Anion					
O1,O2	-0.570	O3,O4,O5,O6	-0.300	C9	-0.150
C1	0.140	C3,C5,C7	0.050	C10,C11,C12	-0.300
C2	-0.050	C4,C6,C8	-0.050	H	0.100

(a) Bond Parameters

Bond	k_b[kJ/(mol •Å^2)]	r_0(Å)	bond	k_b[kJ/(mol •Å)^2]	r_0(Å)
O_w-H_w		1.000	C-C	1351.1465	1.526
C_c-O_c		1.149	C-O	1143.8338	1.425
N_a-H_a		1.010	C-F	2076.6528	1.363
C^--O^-	2260.8720	1.250	C-H	1426.1000	1.105
C^--C	1185.2513	1.520			

(b) Angle Parameters

Angle	k_θ [kJ/(mol •rad^2)]	θ_0(deg)	Angle	k_θ [kJ/(mol •rad^2)]	θ_0(deg)
O_w-H_w-O_w		109.50	O-C-C	293.0760	109.50
H_a-N_a-H_a	146.4400	109.47	C-C-C	195.1049	110.50
O^--C^--O^-	607.0860	123.00	F-C-C	414.4932	107.80
O^--C^--C	284.7024	120.00	F-C-F	397.7460	107.80
C^--C-O	293.0760	109.50	C^--C-H	188.4046	109.50
C^--C-F	414.4932	107.80	H-C-O	238.6477	109.50
F-C-O	397.7460	107.80	H-C-C	185.8940	110.00
C-O-C	251.2080	109.50	H-C-H	165.3790	106.40

[a]w stands for water, c stands for CO_2, and a stands for NH_4^+ cation. C^- stands for carboxylate carbon, O^- stands for carboxylate oxygen, C stands for alkyl carbon, O stands for ether oxygen, and H stands for surfactant hydrogen.

Table 3.1 (con'd)
(d) Dihedral Parameters

Dihedral	A[kJ/(mol•rad)]	ϕ_0	m
-C⎯C-	0.0000	0.0	0
-C-O-	1.6328	0.0	3
-C-C-	5.9557	0.0	3

(e) Improper Dihedral Parameters

Dihedral	B[kJ/(mol•rad)]	χ_0	n
O^--O^--C^--C	48.5669	180.0	2

(f) van der Waals Parameters

Atom type	σ_{ii}(Å)	ε_{ii}(kJ/mol)	Atom type	σ_{ii}(Å)	ε_{ii}(kJ/mol)
O_w	3.165	0.650	O^-	2.860	0.955
H_w	0.000	0.000	C^-	3.617	0.620
C_c	2.757	0.234	C	3.474	0.670
O_c	3.033	0.669	O	2.860	0.955
N_a	3.250	0.712	F	3.081	0.288
H_a	0.000	0.000	H	2.449	0.159

angle bending potential, dihedral potential, and improper dihedral potential respectively. Here k_b, k_θ, A and B are corresponding bond and angle force constants. We also have r_0, θ_0, ϕ_0 and χ_0 as equilibrium bond lengths and angles. In CVFF, the model parameters are optimized based on full 1-4 vdw and electrostatic interactions.

To understand the difference between PFPE and PE surfactants and the relative contributions of total free energy, we performed several computational experiments. In these

experiments we changed various parameters in the surfactant force field to observe the influence due to the changes in electrostatic interaction, Lennard-Jones interaction, and the molecular geometry. We performed a number of simulations where we varied the parameters in the force field from the ones describing PFPE to the parameters describing PE or vice versa. We observed that the data looked especially clear when we considered simulations with only two "artificial" surfactants. The first artificial surfactant had the same bonded parameters as PFPE and the same nonbonded parameters as PE. We called this surfactant molecule A1 in the paper. The second artificial molecule, A2, had the same bonded parameters as PE and the same nonbonded parameters as PFPE. Here bonded parameters refer to various parameters in (3.4) and nonbonded parameters are those LJ parameters and partial charges in (3.2).

The cubic simulation box of micellar simulations contained 66 surfactants, 554 water molecules and 6359 CO_2 molecules. The constant pressure (20 MPa) NPT ensemble was used for all simulations. All simulations were started from random initial configurations and during the MD simulation run the self-assembly into a reverse micelle was observed. Each simulation lasted 50 ns to ensure that the final configuration is equilibrated. To understand the role of CO_2 solvent, we also performed several simulations in a cell containing no CO_2 molecules. NVT ensemble was used for this kind of simulations.

In our monolayer simulations the systems contained 196 CO_2 molecules, 324 water molecules, and 9 surfactant molecules. The cubic simulation box contained water and CO_2 regions. Because of the periodic boundary conditions two interfaces were present in the system. One interface is between water and $scCO_2$, the second interface is also between water/$scCO_2$, only modified by the presence of nine surfactant molecules. A snapshot of a

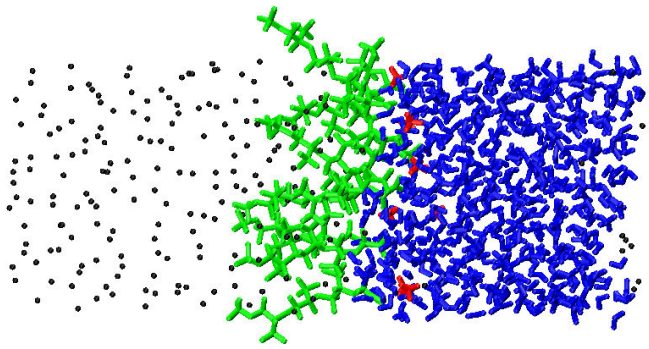

Figure 3.2: Snapshot of PFPE monolayer simulation at t=15 ns. Blue particles are water molecules, green ones are surfactant molecules, red ones are NH_4^+ cations, and black ones are CO_2 molecules.

simulation with a PFPE monolayer is shown in Figure 3.2. All simulations were performed under constant normal pressure and constant surface area (NP_nAT) ensemble and the normal pressure P_n along the *z* axis was equal to 20 MPa, the same pressure as in our micellar simulations [78]. The cross section A in the xy plane was chosen in such a way that the area per headgroup in monolayer simulations was the same as the one in the PFPE micelle simulation (69.5 $Å^2$). The initial configuration of the monolayers we simulated had nine carboxyl carbons of the surfactant headgroup initially distributed on a lattice in the xy plane of the interface and all surfactant molecules in trans conformations.

Each simulation lasted 30 ns: 10 ns of these were spent on equilibration and 20 ns on

data collection. We used the pressure difference formula [73] to calculate the surface tension of each surfactant-modified interface. Since there are two interfaces in each simulation box we subtracted the surface tension calculated for the CO_2/water interface from the total surface tension to obtain the surface tension of the monolayer [19].

In all simulations the temperature was 298.15 K and the time step was 2 fs. The long-range forces were calculated by using the Particle-Mesh Ewald [22] with a cut off for the direct Coulomb interaction and van der Waals interaction having a value of 0.9 nm. The constant pressure was maintained by coupling to the Parrinello-Rahman barostat [64, 65] and the constant temperature by coupling to the Nose-Hoover thermostat [32, 63]; both coupling constants were 0.5 ps. All simulations were performed with the GROMACS MD package [4, 47].

3.2 Results and Discussions

3.2.1 Micellar Simulations

Micelle in CO_2

The most important difference between PFPE and PE micelles is the big exposure to CO_2 on the PE micellar surface (Figure 2.6). In Chapter 2, we have tried to change the area per headgroup by changing the micellar size and keeping the number of surfactant molecules constant. In each simulation we found that the PE molecules tended to come together and formed a cluster. As a result an area of direct contact between CO_2 and water appeared. On the contrary the PFPE molecules tended to keep a distance from each other and formed a uniform distribution on the micellar surface. The uniform distribution of PFPE surfactants on the surface largely decreased the direct contacts between water and CO_2 phases. Thus the surface tension decreased dramatically, which helped to stabilize micellar aggregation thermodynamically. In Table 3.2 we listed the solvent accessible surface area (SAS) of the water core (including NH_4^+) of PFPE and PE micelles. From these data we can see clearly that PFPE has an ability to lower the SAS of water core to a very low value. These results are also consistent with the previous simulations using EMP2 CO_2 model[78].

Our simulations show that the distribution of surfactant on the micellar surface is the key to determine the different stability of micellar systems. The distribution is related to the area of direct water/CO_2 contact which is import in determining the surface tension. A small direct water/CO_2 contact is also thought to be necessary for good surfactants (Stone et al.

[83]).The area per head groups is the same for both fluorinated and hydrogenated surfactants in calculations of Stone et al. [83] Based on this assumption the van der Waals volume of the surfactant determines the water/CO_2 direct contact. We observed in our micellar simulations that the distribution of the surfactants on the interface which is related to the area per headgroup was also a very important factor in determining the water/CO_2 direct contact. Obviously the average distance between surfactant molecules is mainly dependent on the surfactant-surfactant and surfactant-CO_2 interactions. In our PFPE and PE cases we will show that the tail property is an important factor in determining surface activity. In the PE base reversed micellar system the non-uniform distribution of the surfactants produced a "hole" in the direct water/CO_2 contact and the total solvent accessible surface area (SAS) of aqueous core increased largely. Also the PFPE surfactants are uniformly distributed with a larger area per headgroup. The PFPE molecules can better cover the micellar interface with a smaller SAS of aqueous core. The solubility of surfactant tails was also studied by means of SAS of the surfactant anion (in micellar configuration). We believe that SAS is a better index of solubility than the total number of CO_2 in the surfactant layer due to the non-uniform distribution of PE surfactants. In PE micellar system some CO_2 molecules, which are in the surfactant layer, are not located in the solvation shell of any surfactant molecule. The results of SAS for the surfactant anion show that there are more CO_2 molecules having contact with the PFPE surfactant. This result is consistent with the previous results from our group in which the average number of CO_2 molecules in the solvation shell was studied. We noticed that though PE molecules have smaller van der Waals volume, there is less space between PE tails to accommodate CO_2 because of the extreme small average distance between surfactant molecules.

Table 3.2: Accessible surface area of the aqueous core and surfactant anions.

Surfactant in the system	ASA of the aqueous core ($Å^2$)	ASA of surfactant anion ($Å^2$)	Total surface area of the aqueous core ($Å^2$)	Percentage of the exposure of the aqueous core
PFPE	497 ± 114	17863 ± 590	6835 ± 162	7.3%
PE	2049 ± 93	9206 ± 216	6201 ± 101	33.0%
A1	363 ± 78	13622 ± 419	6857 ± 156	5.3%
A2[a]	1858 ± 150	7642 ± 256	6993 ± 195	26.6%
PFPE (in vacuum)	1252 ± 245	11410 ± 348	7361 ± 267	17.0%
PE (in vacuum)[a]	3311 ± 199	5751 ± 131	7958 ± 224	41.6%
A1 (in vacuum)	2619 ± 193	8058 ± 205	8726 ± 248	30.0%
A2 (in vacuum)[a,b]	2696 ± 184	6502 ± 131	7602 ± 185	35.5%

a The simulation started with preassembled micelle configuration.
b During simulation the configuration changed frequently between spherical and wormlike configurations. We chose 1 ns when the micelle was basically spherical to do the ASA calculation.

We also performed micellar simulations for A1 and A2 molecules to confirm our conclusion from monolayer simulations. For A1 molecular system, we obtained the typical reverse micelle similar to the PFPE system. For A2 system we simulated the system for 50 ns and could not obtain a reverse micelle. The final configuration looked like a bilayer. When we started the simulation from an initial spherical micelle, we obtained a micelle with a big exposure to CO_2 in a final configuration. As we will show later on, the simulations of artificial surfactant based monolayer and micellar systems are consistent. All the results of SAS are showed in Table 3.2.

Micelle in vacuum

To understand the role of the CO_2-tail interaction, we performed several simulations for micelles in vacuum and compared them to results from micelles in CO_2 simulations. During the simulations we found that the micelle self-assembled starting from a random configuration. This indicates that in our micelle self-assembly the role of CO_2 was providing friction only. We compared the results for the micelle in CO_2 and that in vacuum for the same micelle, and found that the average surfactant-surfactant distance was smaller in the system in vacuum. This time even PFPE micelle had a small exposure. But the exposure for PE was much larger. The difference between fluorinated and hydrogenated systems still was big. Since we observed the difference between PFPE and PE without CO_2, we think that the interaction between surfactants and CO_2 molecules is not the critical factor determining a difference in the surface activity. But the CO_2 did play a role in simulations. That is to make the surfactants' distribution more uniform and increase the area per headgroup. For PFPE surfactants, the presence of larger surfactant-surfactant distance helps CO_2 molecules to enter

the space between the tails. The CO_2 molecules enter the tail region and push surfactants apart. Thus we observed a uniform distribution of PFPE surfactants in water/PFPE/CO_2 system. On the contrary, the PE tails are too close to each other due to the tail-tail attraction. There are only a limited number of CO_2 molecules which can enter the space between tails. After the CO_2 comes in, the average distance between PE molecules also becomes larger. But the effect is not big enough to make a uniform distribution of PE in water/PE/CO_2 system. This explanation is consistent with the fact that we observed the uniform distribution for PFPE system within a wide range of area per headgroup. In these cases the CO_2 molecules between tails help to create a uniform distribution of PFPE headgroups. What is more, it also can explain the high solubility of fluorinated surfactant in CO_2.

3.3.2 Monolayer Simulations

Surface tension calculations

The ability of certain surfactants to decrease the surface tension of the interface can serve as an index of the efficiency of these surfactants. Usually the value of the surface tension reduction, γ_0-γ (γ is the surface tension in the presence of the surfactant molecules; γ_0 is the surface tension for the pure liquid/liquid interface) depends on a surfactant concentration. At a particular concentration, the large value for the surface tension reduction stands for high surfactant efficiency. Since PFPE is an efficient surfactant, we expect that the simulated system containing the PFPE modified $scCO_2$/water interface has a lower surface tension than the system containing the pure $scCO_2$/water interface. As we can see from Table 3.3, this is indeed the case for the surface tension of the PFPE modified interface. At the same time we observed that the surface tension of the PE modified interface was even higher than that of the $scCO_2$/water interface in our simulation. Here we notice that the values of the surface tension in our simulations are higher than the values from other simulations reported in the literature [12, 13]. Comparison with the results from a simulation performed on a system containing pure $scCO_2/H_2O$ interface, with CO_2 modeled by a three-site EPM2 model [27], showed that the increase in the value of surface tension is due to the single-site CO_2 model that we used. Note that our simulation is performed at a slightly lower temperature compared to the one in the simulation of da Rocha et al. [12], which may also be the reason for the higher value of our surface tension. Although it is nice to obtain in simulations the values for the surface tension that are close to the experimental one, our main interest in this work is to observe the trends in the change of these values as we add different surfactants to

the $scCO_2/H_2O$ interface. Since in our simulations the PFPE modified interface has a lower surface tension compared to the $scCO_2$/water interface, we therefore conclude that our model of PFPE is a model of a "good" surfactant. As we can also see from Table 3.3, the presence of PE surfactant produces a slight increase in the surface tension of the interface with the surfactant compared to the surface tension of the pure interface. This means that in our system containing the PE monolayer, the surface pressure of the monolayer is negative and the monolayer will shrink, if the external pressure is not applied. Such shrinkage of the monolayer is consistent with the creation of a "patch" we observed previously in our micelle simulations [48, 78]. Both the negative surface pressure and the "patch" in the micelle will not be observed in experiments where the surfactant concentration and the size of the system are very different. The slight increase (or at least no reduction) in the surface tension of the interface we observe in the presence of the PE surfactant is the signature of a "bad" surfactant.

What is the reason that PFPE is a "good" surfactant and PE is a "bad" surfactant? To answer this question, first notice that the surface pressure and the free energy of the system containing a monolayer at the liquid water/liquid CO_2 interface can be written as:

$$\pi = \left(\frac{\partial F_m}{\partial a} \right)_{T,n_m} \tag{3.5}$$

$$F_m = n_m \phi_m(a) = n[\phi_{hyd}(a) + \phi_{\text{int}}(a) + \phi_{m-u}(a)] \tag{3.6}$$

where a is the area per surfactant molecule. The three terms in (3.6) are contributions from the headgroup hydration, surfactant interaction (including intramolecular interaction), and surfactant tail-upper phase (CO_2) interaction, respectively. Since the division of the surfactant molecule into the headgroup and tail regions cannot be done uniquely, the relative

contribution of the three terms depends on the convention used for the definition of the regions.

We also performed computational tests with artificial molecules A1 and A2. After we performed our test runs we found that by changing the PE's bonded parameters to those of PFPE's we can produce a "good" surfactant. The CVFF that we use to describe surfactant anions is constructed in such a way that the difference in the bonding parameters describing PFPE and PE is in the values of the bond stretching parameters $k_{b,i}$ and angle distortion parameters $k_{\theta,i}$, and also in the values of the equilibrium bond lengths and angles, while the torsion A_i and the out-of-plane B_i parameters remain the same. The nonbonded term in the energy contains contributions from the Coulomb interaction energy of partial charges and Lennard-Jones interaction energy. The nonbonded parameters for PFPE are different from the ones for PE. As we can see from Table 3.3, the interface with A1 has a surface tension that is lower than the tension for the pure CO2/water interface, and the value of the surface tension is close to that of PFPE. This indicates that A1 is a "good" surfactant. On the contrary, the interface with A2 has a high surface tension, similar to the one with PE. Since the surfactants with the same vdW and partial charge parameters can have very different surfactant performance, we conclude that these parameters are not the only parameters that determine the surfactant performance. As we can see the bonded parameters play a very important role. The conformational distribution of the surfactants also plays an important role. In Table 3.4 we calculated the average tail-tail intermolecular energy (Coulomb plus LJ) using the system trajectories. Here the definition of "tail" incorporates the surfactant molecule without the $-CO_2^-$ group. We can observe from the data that all the energy values are negative indicating that the cohesive energy term plays the dominant role. We observe

that “good” surfactants (PFPE and A1) display a less negative interaction energy compared to “bad” surfactants (PE and A2). This indicates that the conformational distribution of the tails in “good” surfactants is different from that of the “bad” surfactants and that it is possible that tails in “bad” surfactants are in a more condensed state.

To understand the influence of electrostatic tail-tail interactions we also performed simulations with charges on tails removed. Here we used the same definition of “tail” and “head” as in our group’s previous paper [78] (e.g. for the PFPE anion the “head” contained the CO_2^- group, the first CF2 group, and the first ether oxygen). The partial charges on headgroup ether O atoms were modified to keep the whole system at zero net charge. We observed that the big difference between surface tension in systems with PFPE and PE still remained. This fact suggests that our group’s previous conclusion [78] about a strong electrostatic attraction between PE tails may be incorrect. The influence from the tail dipole is very small compared to that of other factors. The influence of the partial charges on the first two PFPE fluorine atoms which can be considered to be part of the headgroup can be seen from the last two rows in Table 3.3. As we can see from this table, the main change in the surface tension is due to the removal of the partial charge on fluorine. The important role of this partial charge is not difficult to understand since the headgroup partial charge can change both the headgroup Coulomb repulsion term and the headgroup hydration term in the free energy expression. We want to emphasize that all our discussions about the role of partial charges are focused on the surfactant-surfactant interactions. The surfactant-CO2 electrostatic interaction is expected to be unimportant for the total free energy as was reported in the literature [25].

Our computational experiments on artificial surfactants indicate the importance of the

Table 3.3: Results for the surface tension calculations[a].

Surfactant on interface	Surface tension (mN/m)
No surfactant	47.6 ± 1.4
PFPE	33.6 ± 2.2
PE	52.2 ± 2.2
A1	38.7 ± 1.4
A2	52.6 ± 0.6
PFPE with no partial charge on tail	29.8 ± 1.5
PE with no partial charge on tail	50.6 ± 2.2
PFPE with hydrogenated head[b]	40.1 ± 0.9
PFPE with no partial charge on first two F atoms	40.9 ± 0.6

a The standard deviation is obtained using a block average method with 4 blocks for each simulation. Here the definition of "head" includes the first $-CF_2$/$-CH_2$ group.
b The first two F atoms LJ parameters and partial charges were changed to those of H atoms on PE.

Table 3.4: The average tail-tail interaction energy for monolayer systems (kJ/mol).

PFPE	PE	A1	A2
-435.03	-555.50	-334.03	-480.24

chain conformations for the effectiveness of the surfactant. Changes in conformations may be accomplished by variation of the Lennard-Jones size parameter, charges, and changes in bonding parameters. We observed that size parameters and partial charges are not the only important parameters that describe the tail-tail intermolecular interactions as one may naively assume and that changes in bonding parameters play a major role in determining the effectiveness of the surfactant. The values of partial charges on the tail atoms do not have a big influence on the surface tension. Partial charges on the first -CH2 or -CF2 groups do have a certain influence.

2D Distribution of Surfactant Headgroups

In our previous simulation of the micellar systems we found that PFPE surfactants uniformly distribute themselves on the approximately spherical $scCO_2$ /water interface in a typical micellar configuration. PE surfactants, on the contrary, tend to cluster together, therefore leaving "patches" where a direct $scCO_2$/water contact on the spherical interface occurs. The results from our monolayer simulations can be linked to these observations, meaning that an effective repulsion exists between PFPE molecules, while an effective attraction should exist between PE molecules. Indeed, we observed a positive surface pressure for the PPFE monolayer, which indicates effective repulsion between molecules and keeps the surfactant distribution uniform. The surface pressure is negative for the PE monolayer, which produces an effective attraction between surfactants and their cluster distribution.

Since we used the same conditions for the micellar and monolayer simulations, we anticipated to see a difference in the distributions of PE versus PFPE surfactants in our

monolayer simulations as well. Although we were not able to observe a patch of direct $scCO_2$/water contact in monolayer simulations, due to a rather small number of surfactant molecules in our simulation box, the analysis showed that the distribution of fluorinated and hydrogenated surfactant in monolayers is different indeed. To understand this difference, we first studied the distribution of the surfactant headgroups. The 2-dimensional radial distribution function (rdf) of the surfactant headgroups is shown in Figure 3.3. The index that denotes the carbon atom in this work is the same as that in our group's previous work [78]. C1 to C9 are backbone carbon atoms starting from carboxyl carbon C1. C10 to C12 are side chain carbons. As we can see from this figure the amplitude of the first peak for the PE surfactant is larger than the corresponding amplitude for the PFPE surfactant, which means that the probability of finding the PE molecules in close contact is higher if compared to the probability for the PFPE molecules. Also, in the PFPE case the amplitude of the first peak is similar to the amplitude of the second peak and both of them are close to unity. This means that the distribution of the PFPE surfactants is more uniform. We also calculated the number of nearest neighbors around the surfactant headgroups. This information is displayed in Figure 3.4. As we can see from this figure, there are more PE headgroup neighbors within a short distance from a central headgroup. This is consistent with a cluster distribution of the PE surfactants.

Because the distribution of the PFPE molecules is uniform, there is, on average, more empty space available between the tails of these molecules. As a result the CO2 solvent molecules can penetrate more efficiently into this space. Therefore we expect that more molecules found in the PFPE's tail region, meaning better solubility of PFPE in CO_2. To check this expectancy we counted the total number of CO_2 molecules in any surfactant's first

solvation shell, as we did in our previous work [78]. As we from Table 3.5 there indeed more CO_2 molecules in the first salvation shell surfactant. This suggests a larger CO_2 penetration into the tail region. We can also observe this penetration from the density profile (Figure 3.5). This figure shows that the density curve for CO_2 drops significantly after entering the tail region for both PFPE and PE cases. Nevertheless, some substantial differences can be seen from the figure; there is a stable region in the PFPE case with a plateau region indicating the CO_2 penetration. On numbers from Table 3.5 and the values of the tail/CO_2 interaction energy, we observe that the conclusion reached previously in the literature that there is no special affinity between fluorocarbon PFPE the basis of the and CO_2 [25] is also applicable in our case. The average tail/CO2 interaction energies in our monolayer simulations are -514.57 and -430.17 kJ/mol for PFPE and PE cases, respectively. If we assume that the interaction is mainly due to CO_2 molecules located in the first solvation shell, we can calculate the interaction energy per each CO_2 molecule in the first solvation shell. The results are -8.30 and -8.60 kJ/mol for PFPE and PE, respectively, meaning that in our simulations the interaction between PE and single CO_2 is approximately the same as the interaction between PFPE and single CO_2. The larger total negative tail/CO_2 interaction energy in the PFPE case is due to a larger number of CO_2 molecules in the solvation shell of the surfactant molecule.

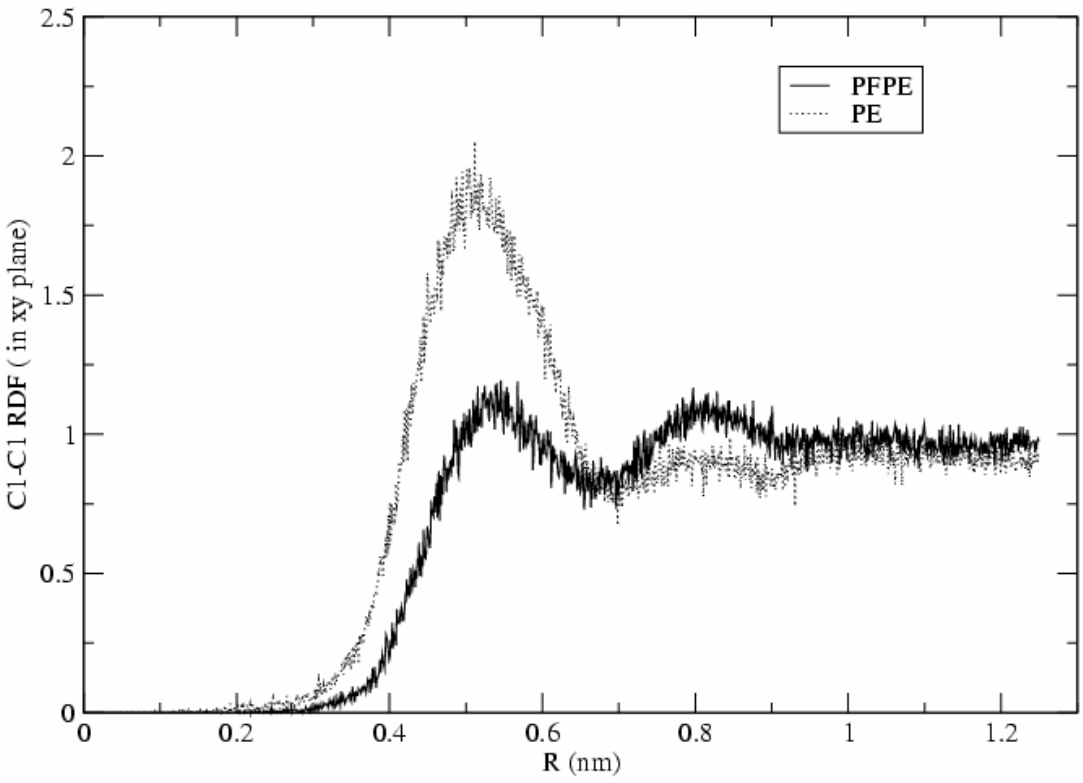

Figure 3.3: Two-dimensional (in xy-plane) radial distribution functions for C1-C1 atoms.

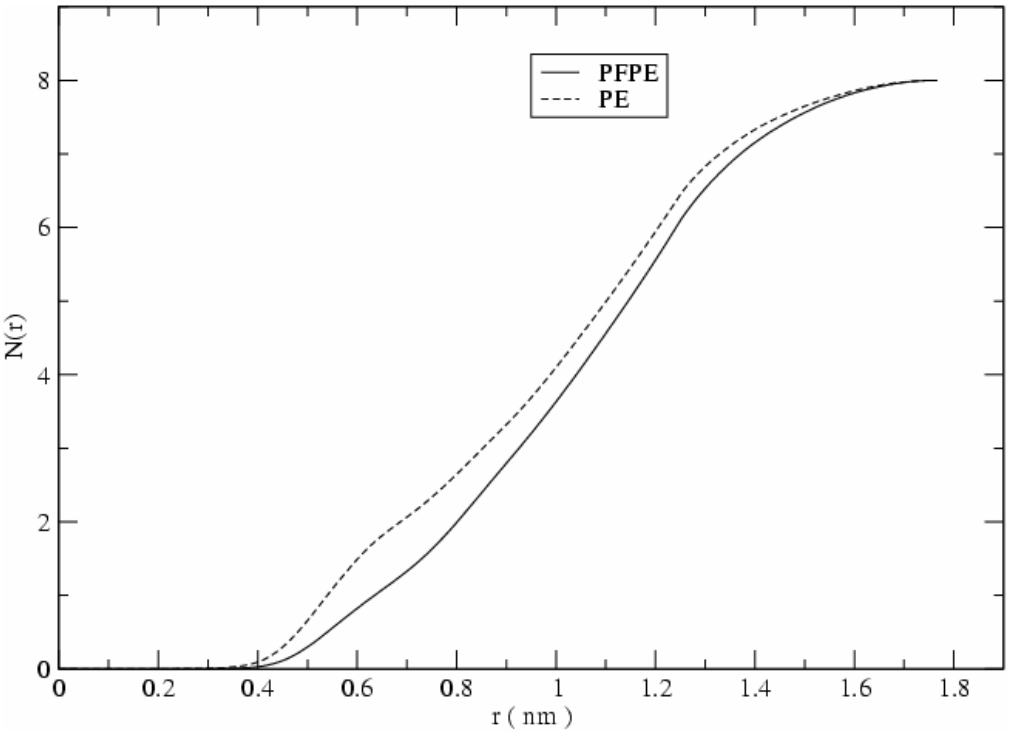

Figure 3.4: Average number of other C1 atoms N® within a distance r from a central C1 atom.

Tail Conformations and Chain Rigidity

As our previous discussion showed, the intermolecular interactions are not the crucial ones that can explain the surface activity of PFPE or PE surfactants. Indeed, as we saw previously, the A1 molecules that have the same intramolecular force field parameters as PFPE and the same intermolecular force field parameters as PE display high surface activity and are "good" surfactants, while A2 molecules that have the same intermolecular parameters as PFPE and the same intramolecular parameters as PE are "bad" surfactants. Intramolecular force field parameters determine the flexibility of the molecules, and consequently, the conformations of the surfactant tails. The strong dependence of the results on the choice of the intramolecular parameters shows that in the case of PFPE/PE surfactants flexibility plays a very important role in the monolayer behavior and its surface activity. Compared to PE molecules, the PFPE molecules are more rigid and they pack and distribute themselves so as to leave more space between tails. The CO_2 molecules can enter this space due to the tail/CO_2 interaction. In their turn the CO_2 molecules push the surfactant molecules away from each other. Thus, we observe that the PFPE surfactants have a uniform 2-dimensional distribution of the headgroups and the system displays a positive surface pressure. The tails of the PE molecules are not so rigid and as a result their conformations are more disordered. The more disordered tails do not leave enough room for the CO_2 molecules to enter. Due to the attraction of the PE tails the surfactants undergo cluster formation. In addition, the CO_2 molecules outside the clusters (in the "patch" region) can also push the surfactants toward each other. As a result, we observe that the PE surfactants display an effective attraction, and a system has a negative lateral pressure in this case.

To check the difference in the conformations of PFPE and PE tails, we performed a

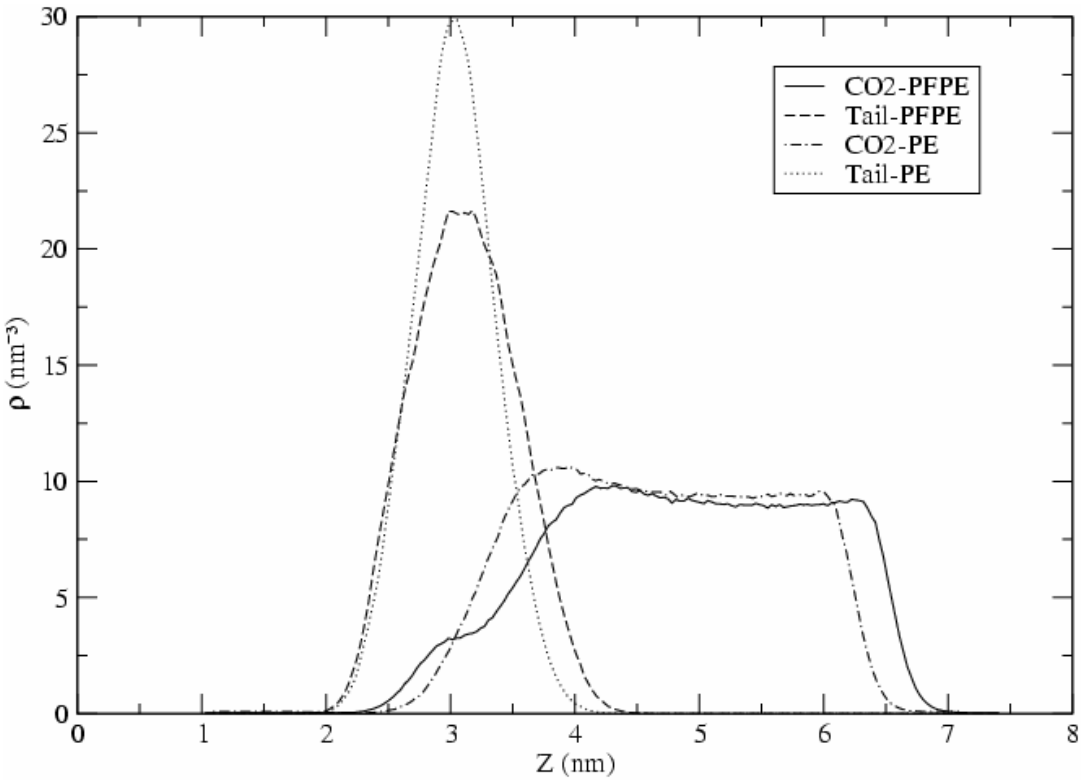

Figure 3.5: Number density for the surfactant tails and CO_2. Each CF_n/CH_n and O was counted as a group.

Table 3.5: Number of CO_2 molecules in the first solvation shell of surfactant tails in monolayer simulations.

	PFPE	PE	PE (headgroup fixed)
Number of CO_2	62 ± 6	50 ± 6	62 ± 5

conformational analysis of our monolayer simulation trajectories. In Figures 3.6 and 3.7 we plotted the number density profiles of backbone atoms with their distances calculated relative to the position of the headgroups C1. Compared to the profile for the PFPE, there are more overlaps seen in the profile of the PE. We also observe broader density distributions in the PE profile, indicating that more disorder is present in the PE monolayer compared with that observed in the PFPE monolayer. The same conclusion on disorder can be obtained from observing the tail density profiles in Figure 3.5. We also plotted the cosine of the angle between the vector connecting C1-Ci and the vector normal in order to study the orientation of each segment in the tail. From Figure 3.8 we observe that the orientation of the PFPE tail is basically perpendicular is an obvious tilt angle for the whole tail. To check the order of each segment, the order parameter

$$S_{CF} = \frac{3}{2} < \cos^2 \theta > -\frac{1}{2} \tag{3.7}$$

(θ is the angle between the CF(CH) bond and the normal to the interface) for each carbon along the chain was plotted in Figure 3.9. As we can see, as the carbon number increases, both PPFE and PE chain segments become more disordered, although the order parameters for the carbons in the PE chains are closer to zero, especially for the last several carbon atoms in the surfactant tails. This confirms the fact that PE tails have a more disordered configuration than PFPE tails. The backbone dihedral trans/gauche ratio can also serve as an important index for the degree of disorder of the surfactant tails. We show in Table 3.6 that the PE tails have a higher percentage of gauche defects which is consistent with our previous discussion. To support our qualitative discussion with a quantitative argument we performed an additional simulation on a PE surfactant monolayer with the headgroup carbon atoms C1 uniformly distributed on a lattice and fixed during the simulation. The results of this

simulation were analyzed and compared with the results of the simulation on the PE monolayer. We calculated the energy and entropy changes for the monolayer tails when going from a system containing the PE monolayer with fixed headgroup atoms to a system with unrestricted distribution of the headgroup carbon the method of Schlitter [77]. As we can see from the data in Table 3.7, there is a negative energy change for the tail/tail interaction when going from a uniform distribution to a cluster distribution, which is caused by the mutual tail approach. Since due to this motion the space between tails is reduced in cluster configuration and the number of CO_2 molecules is pushed out from this space, the number of CO_2 molecules solvating the tail is also reduced, which causes a positive energy change in tail-CO2 interaction. Basically, the two changes cancel each other. The change in tail/aqueous solvent interaction energy is very small and contributes very little to the energy balance. Table 3.7 shows that compared to the energy change, the entropy change is dominant. Thus, the entropic contribution to the free energy change should be considered to be the main driving force for the formation of the cluster configuration.

We also calculated a trans/gauche ratio for surfactants with fixed PE. The result (see Table 3.6) shows that PE monolayer tails are more ordered when monolayer headgroups are fixed in a uniform configuration. These trans/gauche data are consistent with the entropy change. Although this result may seem to be somewhat unusual (surfactant tails usually become more disordered with an increase in the area per surfactant [84]), it can be easily explained. As Table 3.5 shows, the number of CO_2 molecules in the solvation shell of the fixed PE monolayer is larger than that in the unrestricted monolayer. A larger number of CO_2 molecules around the surfactant enforce the surfactant to adopt a more ordered conformation.

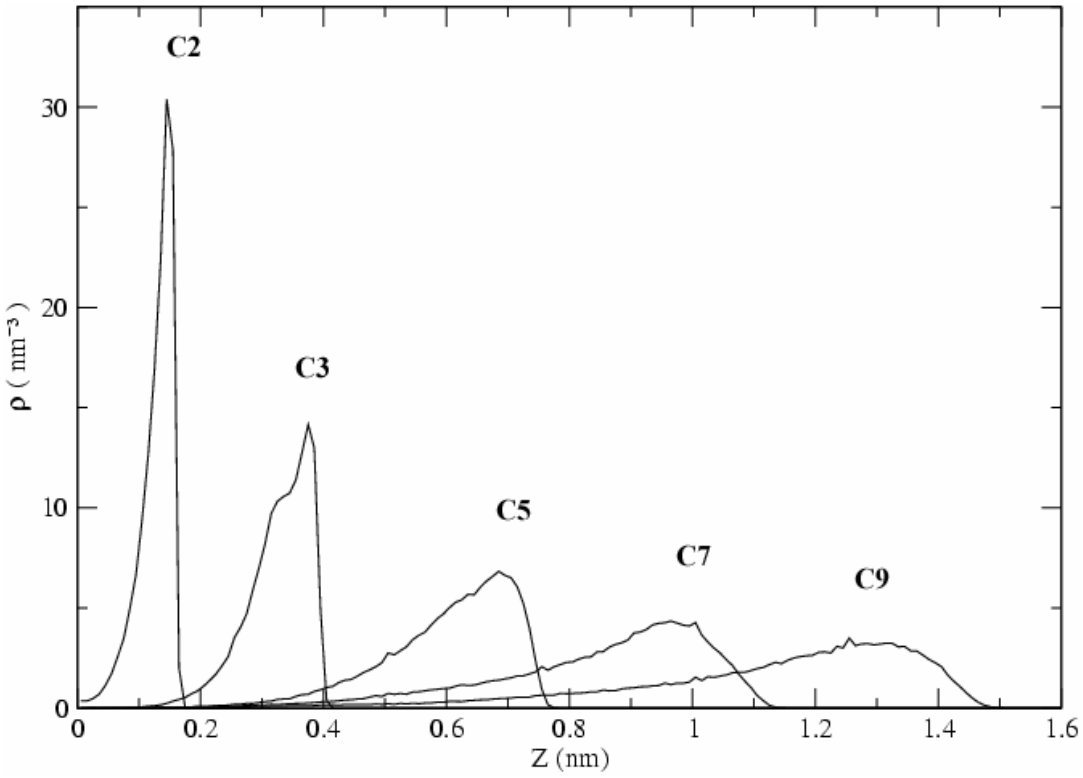

Figure 3.6: Number density for the PFPE backbone carbon atoms as a function of distance to the headgroup.

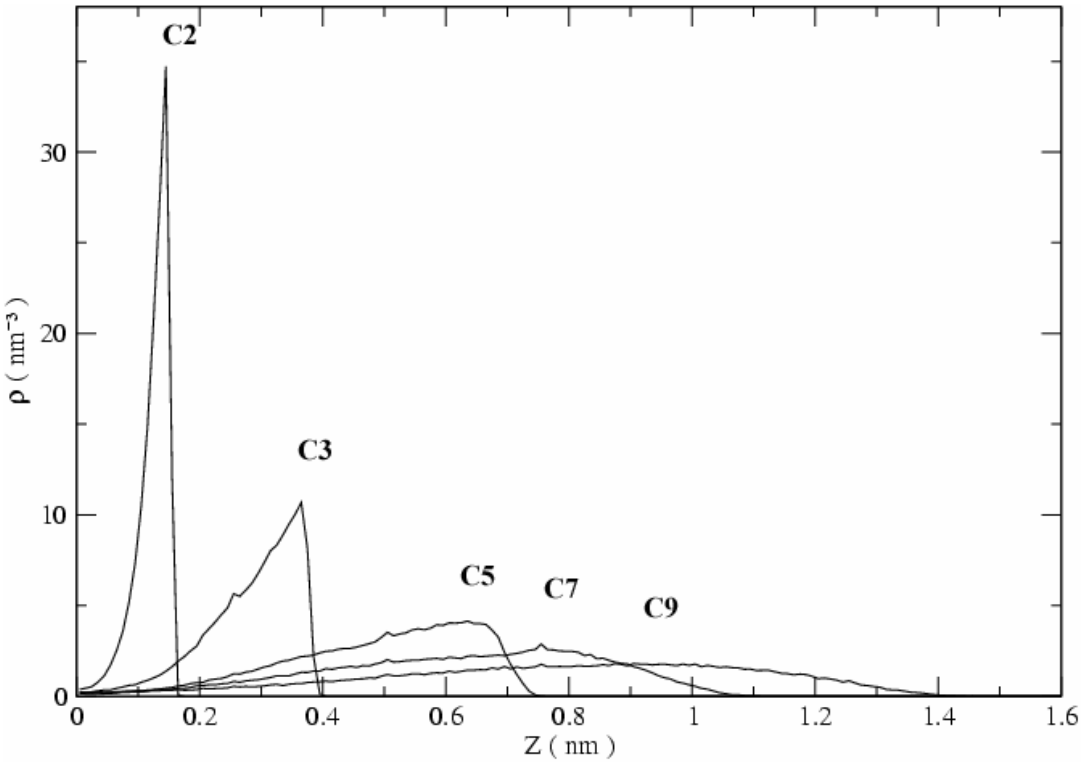

Figure 3.7: Number density for the PE backbone carbon atoms as a function of distance to the headgroup.

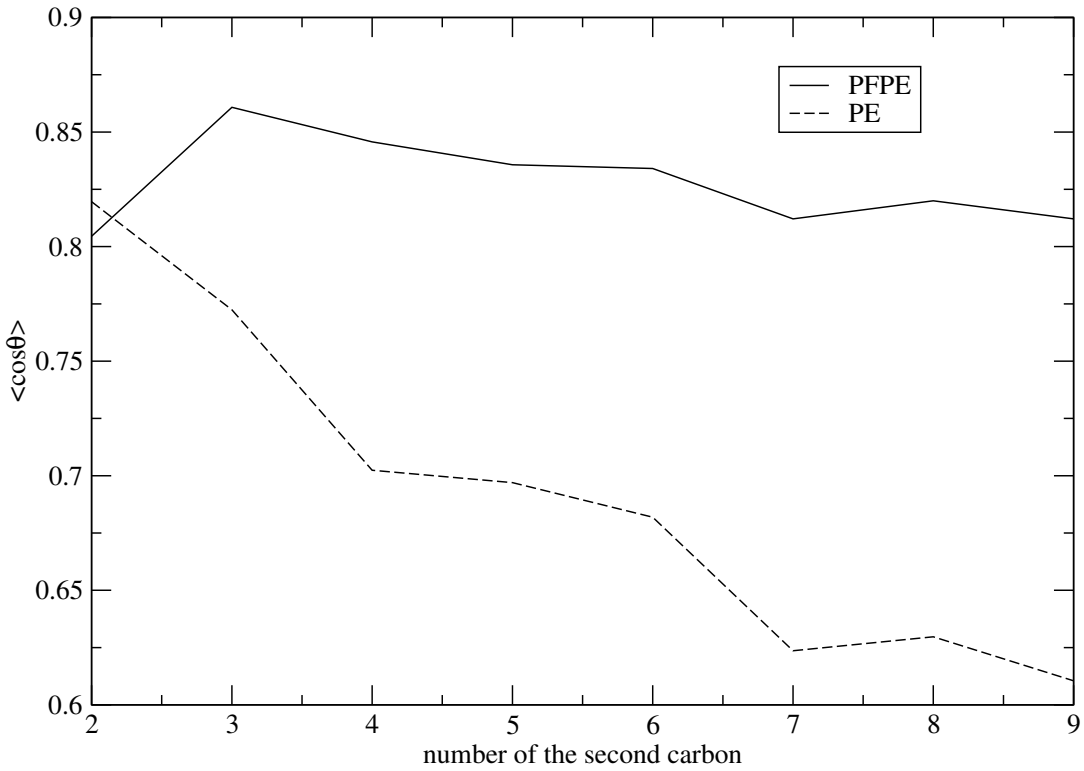

Figure 3.8: The average cosine of the angle formed between the vector normal to the interface and the vector connecting C1-Ci.

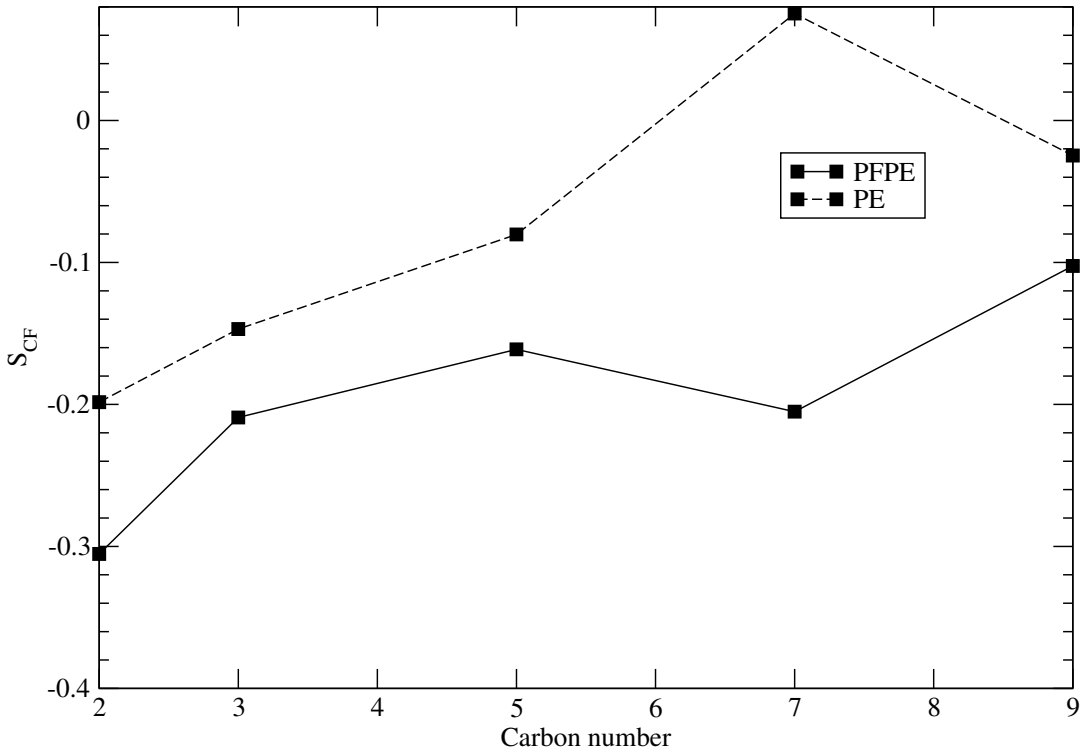

Figure 3.9: The order parameter for the CF(CH) bond.

Table 3.6: The gauche/trans ratio for the surfactant backbone dihedrals in monolayer simulations.

	PFPE	PE	PE with fixed headgroups
g/t ratio	0.296	0.373	0.308

Table 3.7: Energy and entropy change for monolayers when transforming from a state with the PE headgroups fixed to a normal unconstrained monolayer (in kJ/mol).

$\Delta E_{t\text{-}t}$ (tail/tail)	-78.28
$\Delta E_{t\text{-}w}$ (tail/(water+cation))	-1.03
$\Delta E_{t\text{-}c}$ (tail/CO_2)	68.4
$-T\Delta S_{tail}$	-441.32

3.4 Conclusions

We performed MD simulations on systems containing micelles and monolayers of perfluorinated polyether ammonium carboxylate surfactant (PFPE-$COO^-NH_4^+$, MW=695.13) and its hydrogenated analogue PE-COO-NH_4^+ situated at the water/scCO_2 interface to study the difference between the fluorinated and hydrogenated surfactants in order to explain their different surface activity. By changing the force field parameters that are responsible for the relative strength of intra- and intermolecular interactions, we studied the influence of these interactions on the value of the surface tension. We found that intramolecular interactions and molecular geometry play an important role in the surface activity of a "good" surfactant. Our simulation results are consistent with the results from the previous simulations on the reverse micellar systems performed in our group. We observed that the difference in the values of the surface tension for the fluorinated and hydrogenated surfactants corresponds to different 2-dimensional headgroup distributions for the PFPE and PE surfactants. These different distributions are seen in both micellar and monolayer simulations. While in the PFPE case the simulations show that surfactants are distributed uniformly, the PE surfactants are clustering. Various types of analyses were performed in order to reveal the difference in tail conformations of PFPE and PE molecules. We found that the more rigid PFPE tails can provide more space between the surfactant tails for CO_2 molecules to occupy this space. Thus the PFPE tails can be well solvated in CO_2 solvent and as a consequence we observed uniformly distributed PFPE surfactants and the interface had a low surface tension. The more flexible PE tails are more disordered; this leaves less space for the CO_2 molecules to

penetrate between the surfactant tails, thus explaining the low solubility of these surfactants in CO_2. We also performed energy and entropy calculations for the PE molecules when their headgroups were restricted to a lattice configuration on the interface plane. The positive change in the tail conformational entropy for these molecules when going from a restricted to an unrestricted state of motion in the plane of the interface is, in
our opinion, the driving force for the formation of cluster configuration in the PE system. This driving force is not available in the case of PFPE because these surfactants have a rigid tail. How important is this entropic effect for the other surfactant molecules should be a subject of future studies. We feel that the described effect should be considered together with other effects, such as surfactant excluded volume and cohesive energy when designing effective surfactants for $scCO_2$.

Chapter 4

The effect of water structure and surface charge correlations on the hydration force acting between model hydrophilic surfaces

4.1 Introduction

The nature of forces acting between colloidal particles or macromolecules in aqueous solutions is a subject of an intense research activity in material science and biophysics [43, 87]. For charged particles with flat surfaces, a classical DLVO theory [17, 90] that represents interaction forces as a combination of the van der Waals attraction and electrostatic repulsion due to an overlap of double layers can be used as a starting point. The limitations of the DLVO theory are quite clear and attempts were made to improve it by taking into account such factors as, for example, correlations between ions, ion sizes, image forces due to

ion–surface interactions, etc. In addition, there always was an understanding that properties of solvent, and particularly water, must play a role in the inter-particle interaction. Indeed, experiments that studied interactions between neutral phospholipid bilayers demonstratedthat another repulsive force not considered in DLVO theory exists in nature [46]. In an attempt to explain the nature of this force two mechanisms were proposed. One explained the force as due to the restructuring of water at the surfaces and, therefore, this extra to the DLVO force was named the hydration force [45]. Another mechanism did not involve the properties of solvent; it explained the force as due to large scale protrusions of lipid molecules from bilayers and therefore as due to steric interactions between lipids [33]. The fact that an extra non-DLVO force needs to be considered to explain interactions between rigid charged surfaces of inorganic particles such as mica [66] or surfaces of DNA [71] when the protrusions are small indicates that an extra to the DLVO force acting between these particles may indeed contain a component that is due to water. Subsequent experiments performed by McIntosh and Simon [60] on lipid uncharged membranes demonstrated that an extra to the DLVO force due to water also acts between lipid bilayers. Based on experimental measurements, it was also proposed that the hydration force due to water structure can even be of an attractive character [70].

Theoretical work on the nature of the hydration force was initiated by Marcelja and Radic [55]. These authors represented the free energy part due to water encompassed between surfaces in a form described as a series in Landau type expansion. The order parameter in this expansion was not specified and therefore the approach was fully phenomenological. Some of the subsequent theoretical work and simulation work was devoted to the identification and study of this order parameter. Polarization of water between

surfaces represented an appealing choice for the order parameter that should be considered in the problem and therefore some of the initial theoretical work performed by Gruen and Marcelja [26] and by Schiby and Ruckinstein [76] considered the behaviour of this polarization. While the Gruen–Marcelja model used a conjecture that Bjerrum defects constitute the source of the polarization field, Schiby and Ruckenstein proposed that the polarization is caused by the interaction of water with the particle surface and that it propagates due to interacting dipoles of water molecules [76]. Schiby and Ruckenstein considered a homogeneous distribution of water molecules and obtained a smoothly decaying polarization profile. This contradicted the finding from molecular dynamics simulations that showed that polarization oscillated when the surfaces of bilayers were rigid [6]. It was also observed in the simulations that when the restrictions on the motion of a surface group were lifted, the water polarization profile displayed a smooth decay [67]. Subsequently, by considering an inhomogeneous packing of water next to surfaces, Mansiu and Ruckenstein obtained an oscillatory profile for the water polarization embedded between rigid walls [53]. When they considered the surfaces to be rough or fluctuating, the polarization oscillations were removed and a smooth decaying profile was obtained, in agreement with experiments and conclusions from the simulations. The theories that considered the polarization origin for the hydration force used in some or other form the elements of a continuum electrostatic theory and a connection between polarization and the electric field. Recent molecular dynamics simulations of water in Newton black films sandwiched between layers of sodium dodecyl sulphate (SDS) surfactants demonstrated that for water in these films the connection between polarization and electric field has an anomalous character [23]. Simulations also demonstrated that the anomalous response of water polarization to the electric field is

responsible for the strong exponentially decaying short-range repulsion between SDS surfaces [24].

Another class of models considered the disruption and deviation of a water hydrogen bond network from the one found in bulk water as a reason for the hydration force. Attard and Batchelor modelled water between plates to be placed on a two-dimensional square lattice and obtained an expression for the hydration force that depended on a free parameter related to the Boltzmann weight of the Bjerrum defects [2]. Later Besseling generalized the Attard and Batchelor model to three dimensions [7]. In most cases the models considered in the theory of the hydration force represented the surfaces as homogeneous entities. Besseling and in a different model Kornyshev and Leikin [40] considered the effect of the inhomogeneity of the surfaces. As of today only one fully microscopic treatment of a hydration force was performed for a model where large macroions were embedded in a dipolar hard sphere-point ion electrolyte. The integral equations describing the model were solved in the mean spherical approximation [85]. There are also other interesting models related to the nature of the hydration force that can be found in the literature. A brief review of some of these models related to the hydration force is given in the recent work of Valle-Delgado et al. [87]. The strong and weak points of these models are also discussed there together with the comparison between the model predictions and the measurements of the force acting between silica surfaces. It seems that the existing theories cannot fully explain the hydration component of the force acting between silica surfaces. We are not aware of a comparison between predictions of different theories and measurements obtained for forces acting between phospholipid membranes.

Because the study of the hydration force by molecular dynamics (MD) or Monte Carlo

simulation techniques involves the use of a grand canonical ensemble or the presence of a large water reservoir, it requires large computational resources. This is why only a few atomistic simulations of biological or inorganic systems with hydration force calculations are available in the literature [14, 68, 94]. Due to the demanding computer resource requirements in such simulations, the crucial force–distance dependence is obtained for a limited number of data points. Moreover, in the case of simulations with phospholipid membranes, calculated pressures and their components display an appreciable statistical uncertainty. In order to calculate the part of the force that is due to the water structure, as predicted by a large number of theoretical discussions, a more simple model and a more detailed force–distance relationship needs to be obtained in the simulations.

In our recent work [49] we calculated the potential of mean force (PMF) acting between two surfaces represented by a simple model supposed to mimic phospholipid surfaces. In our model the surface was made of a graphene (graphite) plate, electrically neutral, although containing a set of charges to represent dipoles of the lipid headgroups. We will compare the previously obtained PMF data with the prediction from the continuum model and also discuss the free energy component due to the effect of water structure. The detailed analysis of water structure between the plates will also be presented.

4.2 Simulation details

We performed molecular dynamics simulations of two ‘graphene’ plates with artificial

charges which were solvated in 3440 SPC/E water [3] molecules. We calculated the PMFs for a number of different systems. Each system contained two graphite plates that were parallel to the xy plane with a distance r between them. There were 135 carbon atoms in each plate that has a dimension 1.697×1.75 nm. The AMBER 96 force field [11] LJ parameters (σ_{cc}=3.4 Å, ε_{cc}=0.3598 kJ/mol) were used for the carbon atoms. Positive and negative 1.0e charges were uniformly distributed on the plates. Those charges form dipoles with a dipole density around one dipole per 50 $Å^2$. The resulting dipole density on the 'graphene' plates is therefore close to the dipole density in some zwitterionic bilayers and we expect that our simulation results can give some insights into the hydration interaction mechanism between phospholipid bilayers. Our choice of graphene plates was dictated by a fact that the PMF for uncharged plates was already published in the literature [10], so we could check the validity of our calculations for the case when the plates were uncharged. The system containing the uncharged plates can also serve as a reference system, if one wants to study the effect of surface dipoles on the water structure. In Figure 4.1 we showed the simulation box of one simulated the system.

We first repeated the PMF simulation of uncharged system as in the work of Choudhury and Pettitt [10] in order to use the result as the reference state. Then we simulated three types of systems containing a pair of plates and water. Our systems had a different charge correlation between the two plates. The first two types of systems contained a 'plus–plus' and a 'plus–minus' charge arrangement and we called them type A and B systems in our previous work [49]. In the type A system the plate (a) from figure 1 was opposing plate (a) and the charges were in registry ('plus–plus'). In the type B system the plate (a) was opposing plate (b) and charges were in counter registry ('plus–minus'). We also studied here

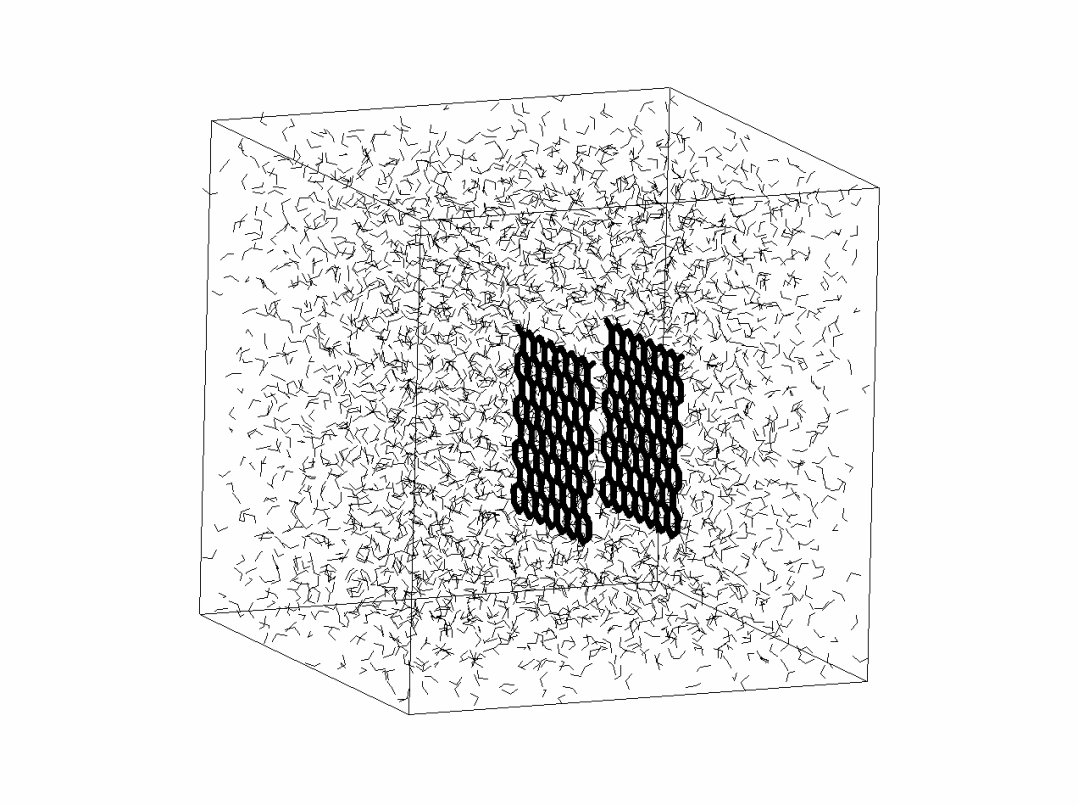

Figure 4.1: A simulated system with an inter-plate distance D=0.92 nm. The system contains two graphite plates solvated in water.

a third arrangement of charges on the plates; we call this arrangement type C. In the type C system the plate (a) is facing plate (c) from Figure 4.2. The charge arrangement in type C system cancels the direct electrostatic inter-plate interaction. We expect that in real membrane systems, the charge correlation between two membrane surfaces might be somewhere between the 'plus–minus' case (type B) and the no obvious charge correlation case (type C). Which case is realized depends on the strength of interactions between charges on opposing surfaces and on the value of thermal fluctuations in the positions of these charges. Leikin [44] proposed that the hydration repulsion dominates when the correlation between charges on plates is small due to their thermal fluctuations; as a result the direct inter-surface interaction is also small. We cannot generate charge fluctuations in our fixed charge model. However, we simulated the type C system to show the possibility of the hydration force domination when the direct electrostatic force is small.

In order to check if the hydrophobic/hydrophilic character of the plate was changed when we added dipoles, we studied the changes in water structure next to plates with and without dipoles. Figure 4.3 shows the density of water as a function of a distance from the plate. As a matter of fact, the distance form the fist density peak to the surface of the plate with dipoles is smaller than the sum of carbon and water radii, indicating that the plate is wetted. This is why we consider the plate with dipoles to be "hydrophilic".

To study the interactions between plates in our three cases we used the thermodynamic perturbation method and calculated the potential of mean force (PMF) acting between the two plates. The inter-plate distance r was used as the thermodynamic parameter that we changed slowly. The difference in Gibbs free energy between two states at different inter-plate distances, r_1 and r_2, can be written as:

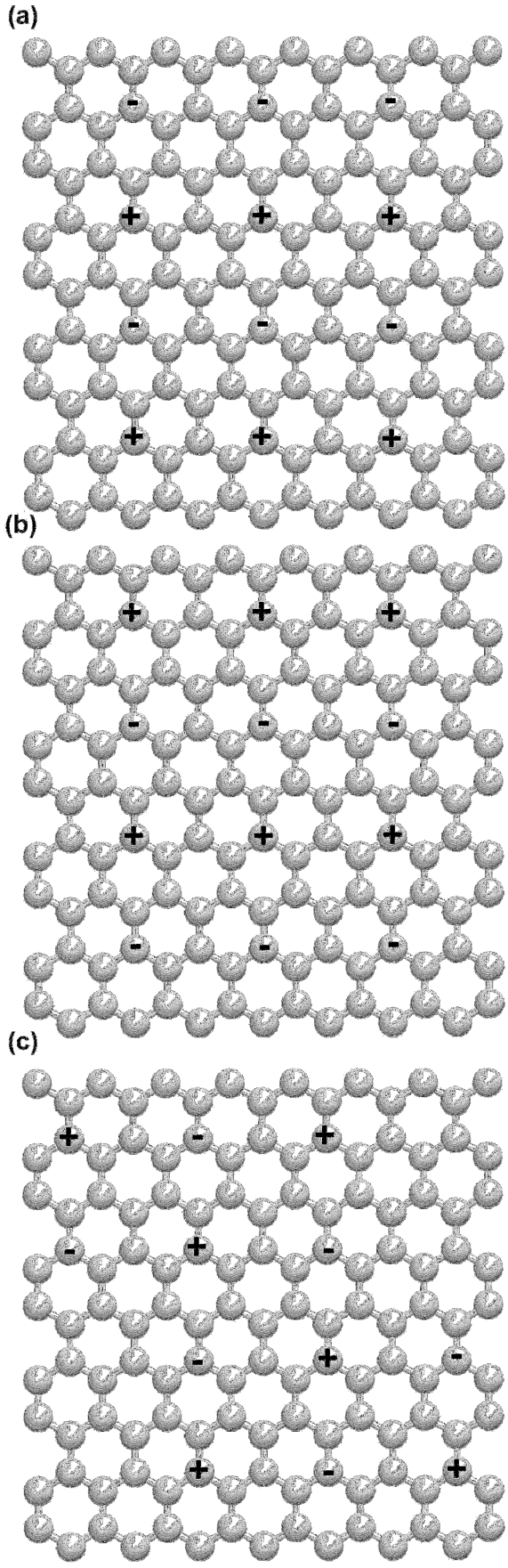

Figre 4.2: Graphene plates with 135 carbon atoms and dimensions 1.697 ×1.72 nm as in type A, B and C systems. Positive and negative 1.0e charges are marked with '+' and '-' respectively. For type A systems, two plates as in (a) oppose each other. For type B systems, one plate as in (a) opposes a plate as in (b). For type C systems, there is one plate as in (a) and another plate as in (c).

$$\Delta G = G(r_1) - G(r_2) = -k_B T \ln \left\langle e^{-[U(r_1)-U(r_2)]/k_B T} \right\rangle_1 \quad (4.1)$$

where U denotes the potential energy of the system. A series of short molecular dynamics (MD) simulations on states with different inter-plate distances, r, were carried out to obtain the corresponding values of the potential energy. Then using equation (4.1) we calculated the free energy change between two adjacent states. We considered two adjacently simulated states with $r = r_i$ and r_{i+1} and perturbed both these states to $r = (r_i + r_{i+1})/2$. Thus we obtained two free energy changes: $G(r_i)$-$G[(r_i+r_{i+1})/2]$ and $G[(r_i+r_{i+1})/2]$-$G(r_{i+1})$. By performing these type of calculations on N simulated states we obtained 2N-2 values of ΔG. Hence, by summing all the free energy changes from the largest separation to a given distance r, we obtained the total PMF corresponding to that inter-plate distance. Here we assumed that the free energy of the system with the largest inter-plate distance r_{max} is zero. More detail on the PMF calculations can be found in the paper of Choudhury and Pettitt [10]. In our present study we used $\Delta r = 0.2$ Å as the smallest inter-plate distance change. For the system with hydrophobic plates, the range of r was from 3.0 to 13.2 Å and there were 52 totally separate simulations performed. For A, B and C type systems, the range of r was from 3.0 to 17.2 Å and 72 separate simulations were done in each case. In order to obtain the solvent contribution into the PMF we used the relation

$$w(r) = w_{sol}(r) + U_{g-g}(r) \quad (4.2)$$

Here the inter-plate potential $U_{g\text{-}g}$ can be easily calculated from the MD trajectory, the W_{sol} is the solvent contribution into the PMF, which we also call hydration interaction. In equation (4.2) $U_{g\text{-}g}(r)$ is the inter-plate potential that can be easily calculated from the MD trajectory and $w_{sol}(r)$ is the contribution from the solvent. An estimate of the solvent effect can also be made by using a simple continuum model. The solvent contribution calculated this way is

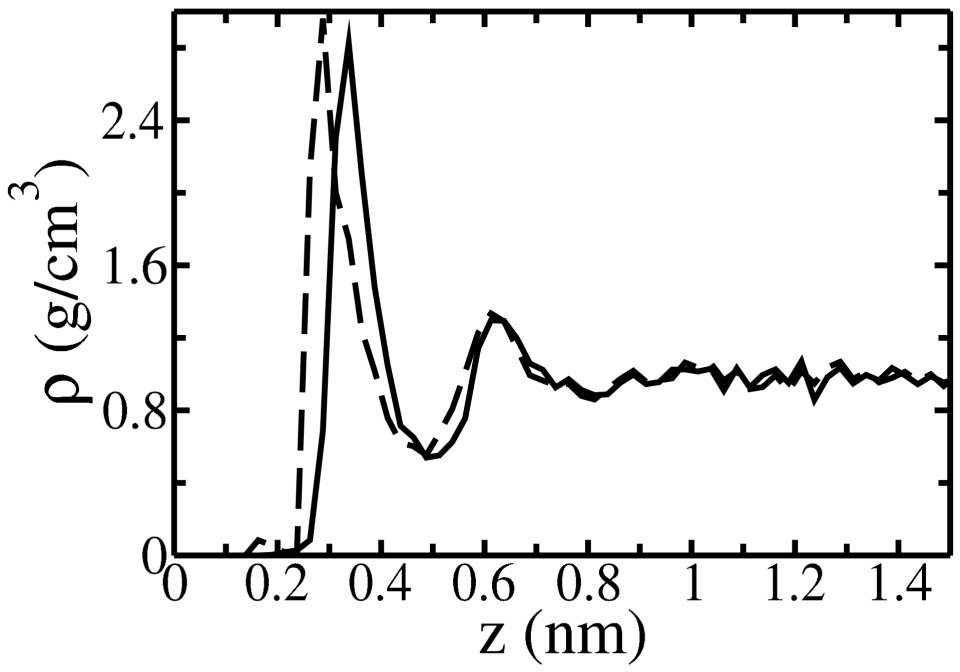

Figure 4.3: Density of water as a function of the distance from the plate. Solid line is for water next to graphite plate, dashed line is for water next to “hydrophilic” plate.

given by

$$w_{sol,c} = U_{elec,c} - U_{elec,g-g} = (\frac{1}{\varepsilon} - 1)U_{elec,g-g} \quad (4.3)$$

Here the two energy terms are electrostatic interaction energy between two plates in water described by a continuum and in vacuum; ε is the dielectric constant of water.

For each system at each value of r we performed a short MD simulation of 1 ns duration with a time step of 2 fs. The first 500 ps of the simulations were used for equilibration and 500 ps for data collection. The NPT ensemble was used for all the simulations with temperature 298K and pressure 1.0 bar. The long-range forces were calculated using particle-mesh Ewald [22] with a cut-off for the direct Coulomb interaction and the van der Waals interaction having a value of 0.9 nm. The pressure and temperature were coupled by the Nose –Hoover thermostat [63] and the Parrinello–Rahman barostat [64, 65] both with coupling constants of 0.5 ps. All simulations were performed using GROMACS MD package [4, 47].

4.3 Results and Discussions

Potential of mean force between two plates

Initially, we calculated the potential of mean force and its components for the system containing uncharged plates. The results _shown in Figure 4.4 are consistent with the results from the work of Choudhury and Pettitt [10]. The PMF shows an oscillatory behavior at distances between 5–11 Å reflecting the size of the water molecules. The two minima at 6.8 and 10.0 Å are at distances corresponding to one and two layers of water molecules situated between the two plates. The inter-plate interaction energy in this case is due to Lennard-Jones interaction only. The contribution from water to the total PMF shows oscillations around zero when *r* is larger than 6.8 Å. When *r* is less than 6.8 Å, water contributes a repulsive component into the total PMF reflecting the need for work to remove water from the last layer between the plates.

The results of PMF for type A, B and C systems are shown in Figure 4.5. The PMF from the type A systems is strongly repulsive because of the large interpolate electrostatic repulsion. The water contribution w_{sol} in this case is attractive in the range of one to two layers of water between plates. For the type B systems the PMF is somewhat flat, while the w_{sol} curve is strongly repulsive. The two PMFs described above and their water components display an oscillating character, when the inter-plate distance is smaller than the distance that two layers of water can fit in. We observe that the direct inter-plate interaction dominates the PMF in both cases because of the very strong electrostatic interaction from perfect inter-plate charge correlation. However, the solvent contribution dominates the PMF from the type C

system, as we can see in Figure 4.5. In this case both PMF and w_{sol} display a strong repulsion at close distances followed by oscillations when the distance is within the distance that two layers of water can be placed between the plates. Therefore, we observe the possibility of a solvent-induced force domination due to a special charge distribution, although the charge distribution here is quite artificial.

In both type A and B cases the PMF contribution from the solvent is always acting in a direction opposite to the direct inter-plate interaction force, i.e. if the direct contribution is attractive the solvent contribution is repulsive or vice versa. This is also the case when the solvent is considered to be a dielectric continuum. In this case the direct interaction can be reduced by the value of solvent dielectric constant and the solvent contribution is therefore given by equation (4.3). We present the solvent contribution based on equation (4.3) along with w_{sol} obtained from equation (1) in Fgure 4.6. A remarkable and somewhat surprising conclusion that one can make from observing the plots in Figure 4.6 is that the simple continuum model agrees quite well with our MD w_{sol} results at distances when more than two layers of water can enter the space between the plates (at distances beyond 10Å). We also observe that our calculated w_{sol} strongly deviates from the continuum prediction at small distances. According to theoretical conclusions [54] and simulation results [91], the value of the dielectric constant of water in the region near the plates should be smaller than the value for bulk water. However, the difference between those calculated from MD w_{sol} curves and the ones predicted by continuum is so large at smaller distances that it is not possible to explain the deviation between the two curves by simple reduction in the value of the dielectric constant. Moreover, in case B the reduction in the dielectric constant will produce an even larger difference between continuum result and MD simulation than the one that

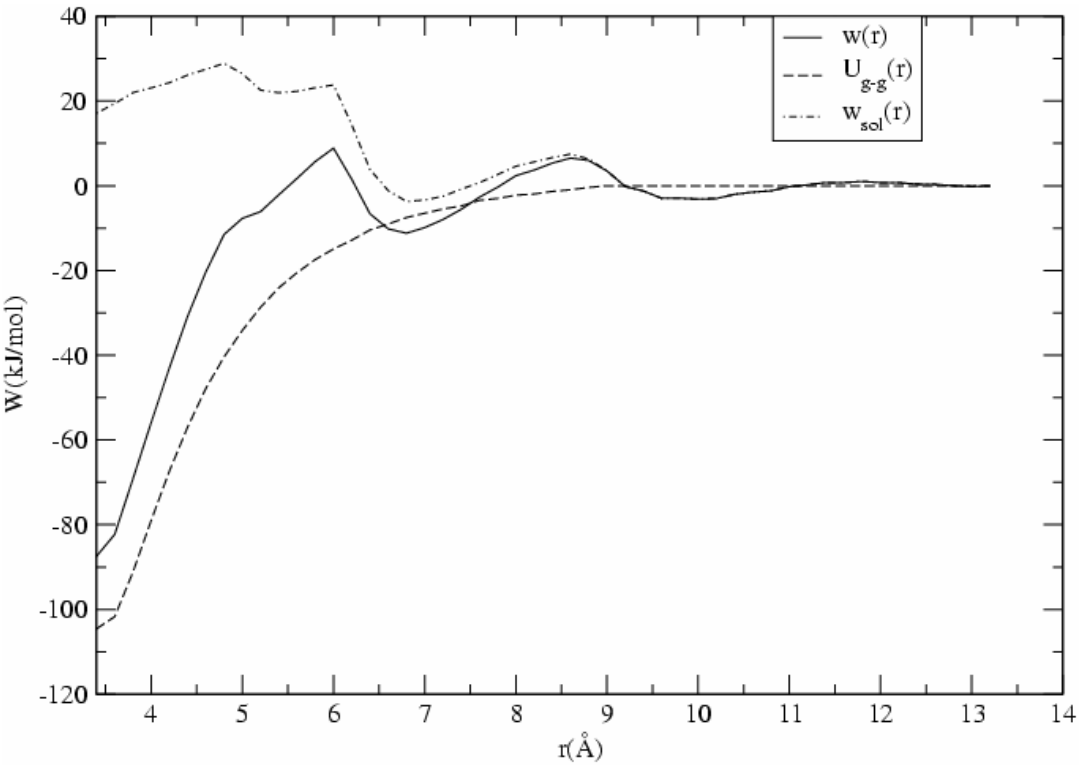

Figure 4.4: The potential of mean force w(r) (solid line), the interaction potential between two graphite plates $U_{g\text{-}g}(r)$ (dashed line) and the solvent contribution $w_{sol}(r)$ (dot-dashed line) for the systems which contain two graphite plates with no charges.

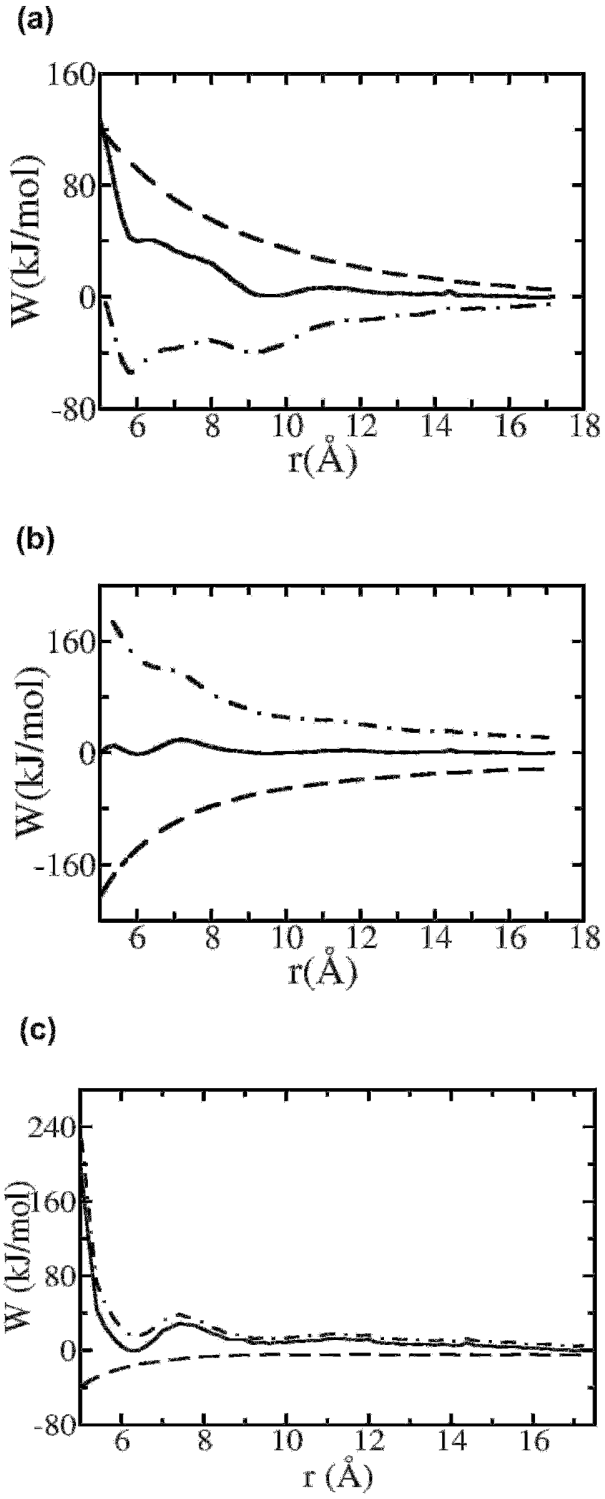

Figure 4.5: The potential of the mean force and its components for: (a) type A systems; (b) type B systems and (c) type C systems. The solid lines are for the total potential of mean force w_{pmf} between plates; the dashed lines are for the direct plate-plate interaction potential $U_{g\text{-}g}$ and the dot-dashed lines are for the potential w_{sol}.

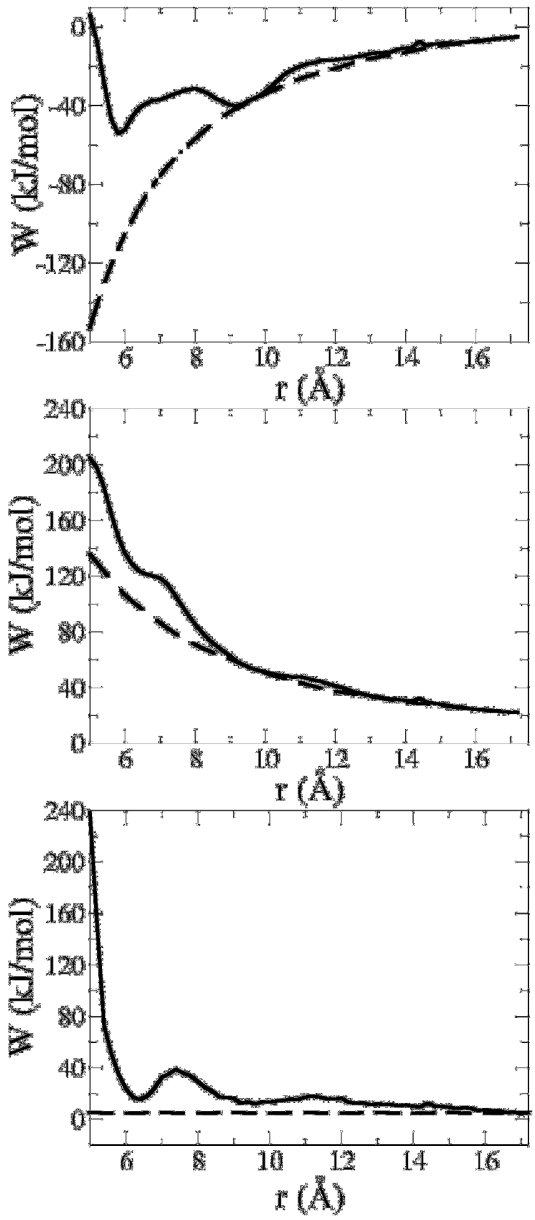

Figure 4.6: Comparison between w_{sol} and $w_{sol,c}$: (a) type A case; (b) type B case and (c) type C case. The solid lines and dashed lines are for w_{sol} and $w_{sol,c}$ respectively.

already exists.

We did not include type C case in our detailed discussion of the connection between the free energy and water structure that is given below, because the arrangement of charges given in the type C system is somewhat artificial. Also, one can get an understanding of the importance of water structure by just considering cases A and B. In order to explain the character of the water contribution into the PMF and the difference between type A and B cases, we performed a systematic analysis of water structure between plates in each case.

Orientational structure of water molecules between two plates

We have calculated the orientational distributions for water molecules situated between the two plates. All calculations are done for distances when there are one or two layers of water molecules confined between plates. These inter-plate distances can be found from the proper minima in PMFs.

We calculated the normalized orientational distributions $P(\cos\theta)$ defined as the probability of finding the cosine of an orientation angle $(\cos\theta)$ in the interval $\Delta(\cos\theta)$ divided by the interval length $\Delta(\cos\theta)$. Here the angle _ refers to the angle between the vector of interest and the z axis. For the water dipole moment, the angle θ is the angle between the water dipole moment vector and the z axis. The θ angle in the OH bond orientation distribution $P_{OH}(\cos\theta)$ is the angle between OH vector and z axis.

By analysing the orientational distributions we can learn about the water structure between plates. For comparison purposes let us first examine the structure of water between uncharged plates. Figure 4.7 shows orientational distributions for water molecules in the case when one layer of water is situated between the non-charged plates. We observe that the most

probable cosine value for both P_μ and P_{OH} is $\cong 0$ which corresponds to a 90_ angle between the OH vector and the z axis and the dipole and the z axis. This result implies that most of the water molecules between the plates are situated in the xy plane. Since there is no electrostatic force acting between water molecules and plates, the orientation of water between plates is mostly determined by the desire of water molecules to maximize the number of hydrogen bonds between themselves. In view of the fact that in our case there is just one layer of water between plates, most water molecules tend to stay in the xy plane. This way they can create the most efficient hydrogen bonding network. The situation with two layers of water is shown in Figure 4.8. As we can see from the figure, the P_{OH} displays sharp peaks located around cosine values of ± 1. These correspond to 0^o and 180^o, indicating that one of the hydrogen atoms points towards the direction along the z axis in an effort to hydrogen bond between the two water layers. The other hydrogen atom of the water molecule is pointed in a direction which is close to being perpendicular to the z axis. This is why we observe a broad peak in P_{OH} around cosine equal to 0. This picture is also confirmed by the observed broad distribution of P_μ, which indicates that to maximize the hydrogen bonding network one needs to have both intra-layer and inter-layer hydrogen bonds. The water snapshots taken at two distances corresponding to the minima in the PMF are also shown in our figures. They confirm our conclusions about the water structure.

The orientational distribution plots and MD snapshots for type A systems with one and two layers of water between plates are shown in Figures 4.9 and 4.10 respectively. Since there are layers of water that are enclosed by negatively charged portions of the plates and layers enclosed by positively charged portions, we expect to see the signature of this arrangement in the distributions. Indeed, we notice from the snapshot given in Figure 4.9(c)

that planes of water molecules are either parallel to the yz plane or parallel to the xy plane. First consider a water molecule located in the yz plane with its dipole moment vector perpendicular to the z axis. In this case we find that angles θ between the OH vectors and the z axis are $\sim 35^{o}$ and $\sim 144^{o}$. These angles explain why the observed peaks for POH in figure 6 are at the values of cosine = ±0.8. Therefore we conclude that water molecules situated between negatively charged portions of the plates have their molecular planes oriented parallel to the yz plane with their dipole moment μ perpendicular to the z axis. This will maximize favourable electrostatic interactions between positively charged hydrogen atoms of water molecules with the negatively charged portions of the plane. However, water molecules between portions of the plates containing positive charges prefer to stay in the xy plane to avoid direct contacts between hydrogen atoms and plate positive charges. For these water molecules the vectors along the dipole moment and along the direction of the OH bond are perpendicular to the z axis and this is why we observe peaks at $\cos\theta = 0$ in the distribution functions. These arguments explain why in the case when only one water layer is present in system A, the distribution of P_{μ} is centred around the value of 0 and the most probable angles for the P_{OH} distributions have their cosine values of 0 and ±0.8. Because water molecules in the layer can be found in two planes, the hydrogen bonding network in water is largely destroyed. We can also observe from the snapshot that some hydrogen atoms of water molecules located near the plate negative charges have close contacts with each other. This is energetically unfavorable for water– water interactions, but energetically favorable for water plate interactions. Notice that in the region between two positive plate charges it is not possible for a water molecule to form close contacts with both negative charges, since there is only one negative oxygen atom in the water molecule.

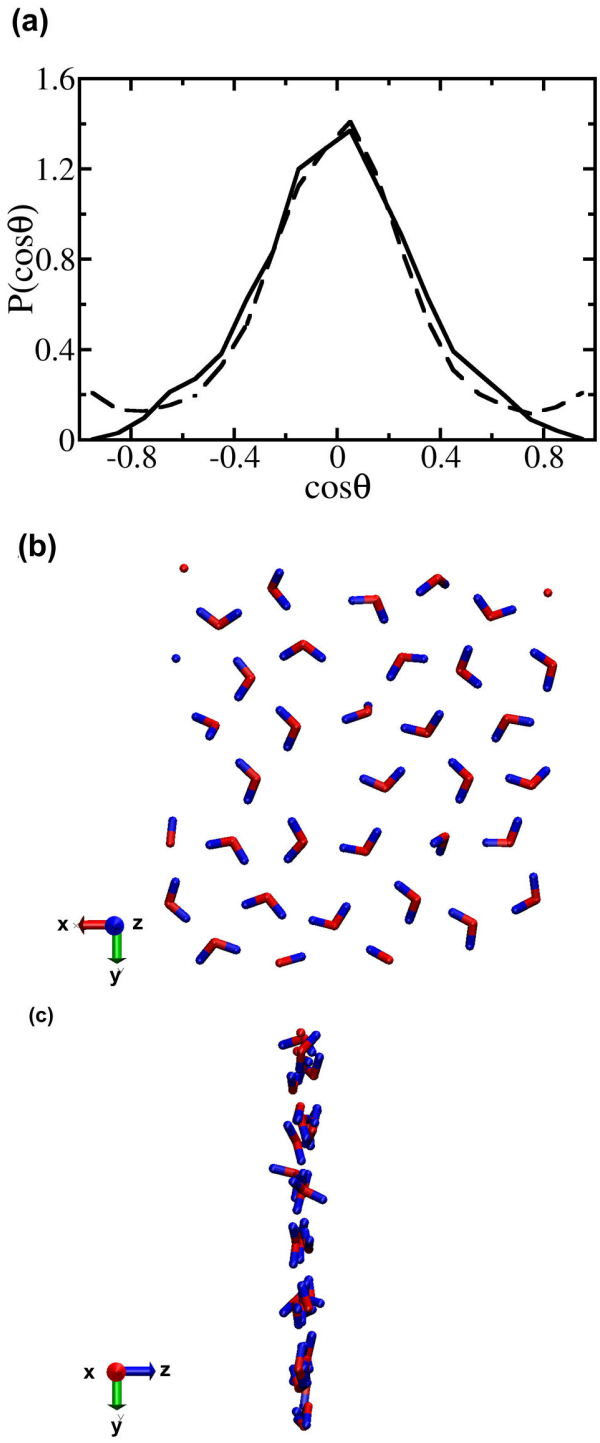

Figure 4.7: (a) Water orientational distributions in the system of non-charged plates with r = 6.8Å. The meanings of θ and P(cosθ) are discussed in the text. The solid line is for $P_{\mu}(\cos\theta)$ and the dashed line is for $P_{OH}(\cos\theta)$. (b) The snapshot of water molecules; view from the xy plane. (c) The snapshot of water molecules; view from the yz plane. Oxygen atoms are red and hydrogen atoms are blue in all the snapshots in this chapter.

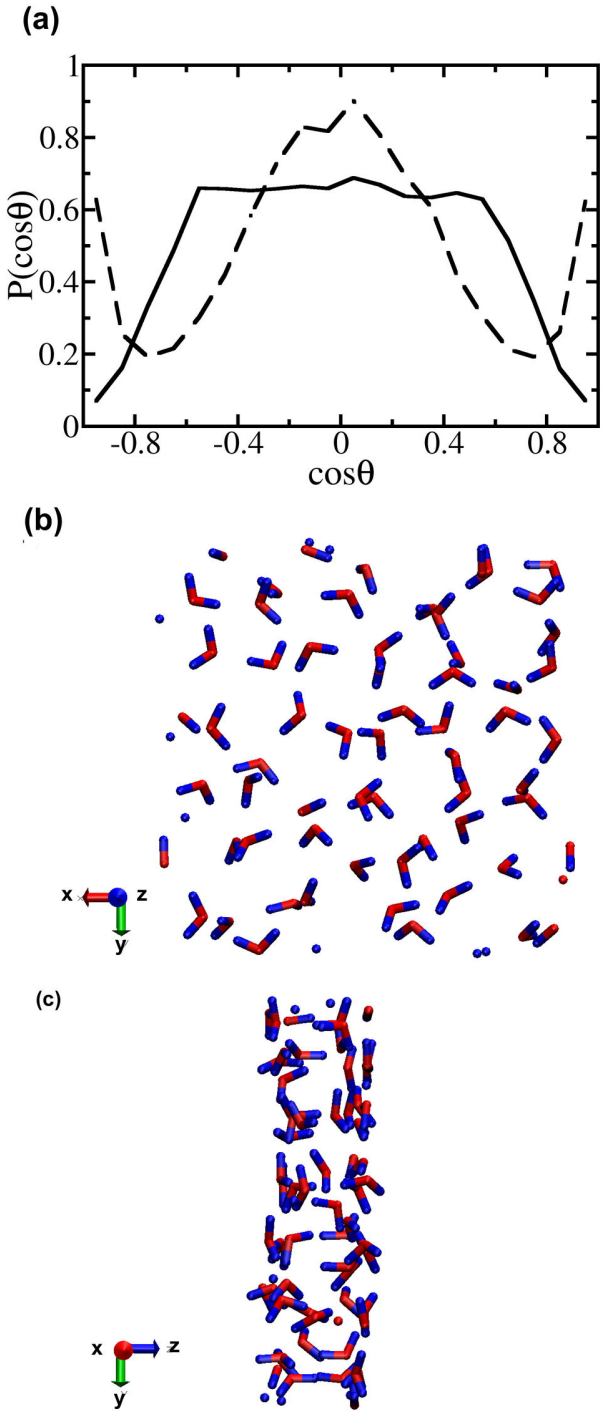

Figure 4.8: (a) Water orientational distributions in the system of non-charged plates with r = 10.0Å. The meanings of θ and P(cosθ) are discussed in the text. The solid line is for $P_{\mu}(\cos\theta)$ and the dashed line is for $P_{OH}(\cos\theta)$. (b) The snapshot of water molecules; view from the xy plane. (c) The snapshot of water molecules; view from the yz plane.

Let us now turn our attention to the case when there are two layers of water between plates in case A (Figure 4.10). Again, by looking at the snapshot from Figure 4.10(c) we conclude that, like in case A with one water layer, water between negatively charged portions of the plates is oriented differently than water between positively charged portions. Consider initially water molecules between negatively charged portions of the plates. Figure 4.11(a) shows the distributions of P_μ and P_{OH} for them. From these distributions we infer that the most probable orientations of water are obtained when one of the water OH bonds is pointing towards the plate and another OH is making an angle 109.4^o with the z axis. This is the origin of the four peaks in POH at values around ±1 and around ±0.3 and of the two peaks at values around ±0.6 for P_μ in figure 4.11(a). A snapshot from the MD trajectory is also consistent with the above discussion. Figure 4.11(b) shows the distributions for water molecules enclosed by positively charged portions of the plates. In this case the distribution of P_μ is more homogeneous, indicating the presence of a more homogeneous distribution of orientations, although some preference is given to orientations with the dipole moment parallel to the z axis, like the snapshots from Figure 4.10 show. Since there are two kinds of regions between plates, what we get in the orientational distribution (Figure 4.10) is the sum of the distributions shown in Figure 4.11. The distributions have a mirror image symmetry because of the symmetry of the system. We notice that the opposite orientations of water molecules due to this symmetry are energetically unfavourable for the interaction between the two layers of water, though it is favourable for water–plate interactions. The hydrogen bonding network is largely destroyed in this configuration.

A similar analysis of water molecular orientations has been done also for the type B systems. The orientational distributions for the case when one water layer is found between

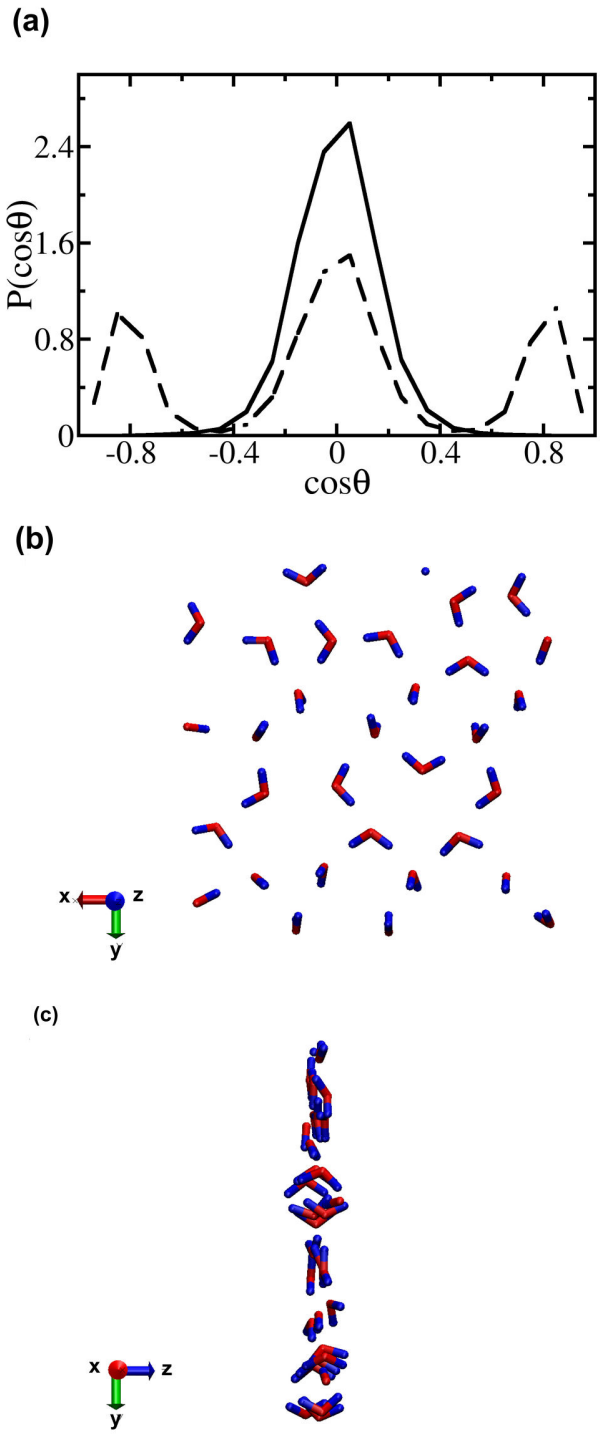

Figure 4.9: (a) Water orientational distributions in the type A system with r = 5.8Å. The meanings of θ and P(cosθ) are discussed in the text. The solid line is for $P_{\mu}(\cos\theta)$ and the dashed line is for $P_{OH}(\cos\theta)$. (b) The snapshot of water molecules; view from the xy plane. (c) The snapshot of water molecules; view from the yz plane.

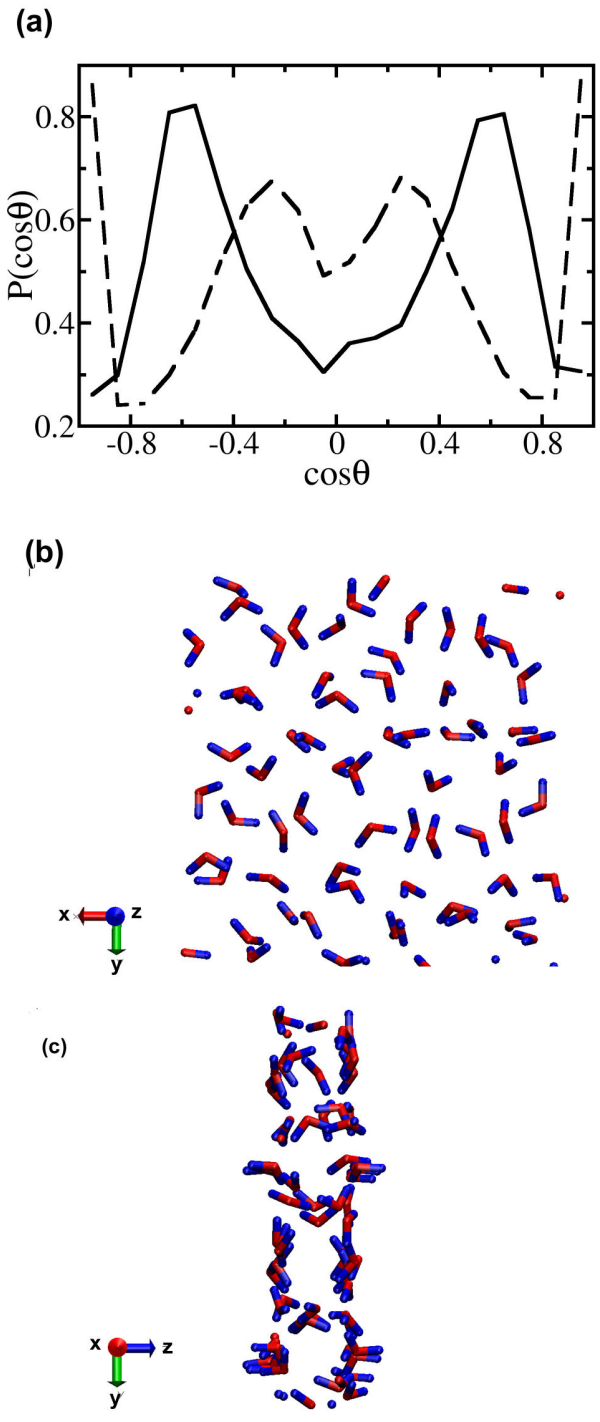

Figure 4.10: (a) Water orientational distributions in the type A system with r = 9.2Å. The meanings of θ and P(cosθ) are discussed in the text. The solid line is for $P_{\mu}(\cos\theta)$ and the dashed line is for $P_{OH}(\cos\theta)$. (b) The snapshot of water molecules; view from the xy plane. (c) The snapshot of water molecules; view from the yz plane.

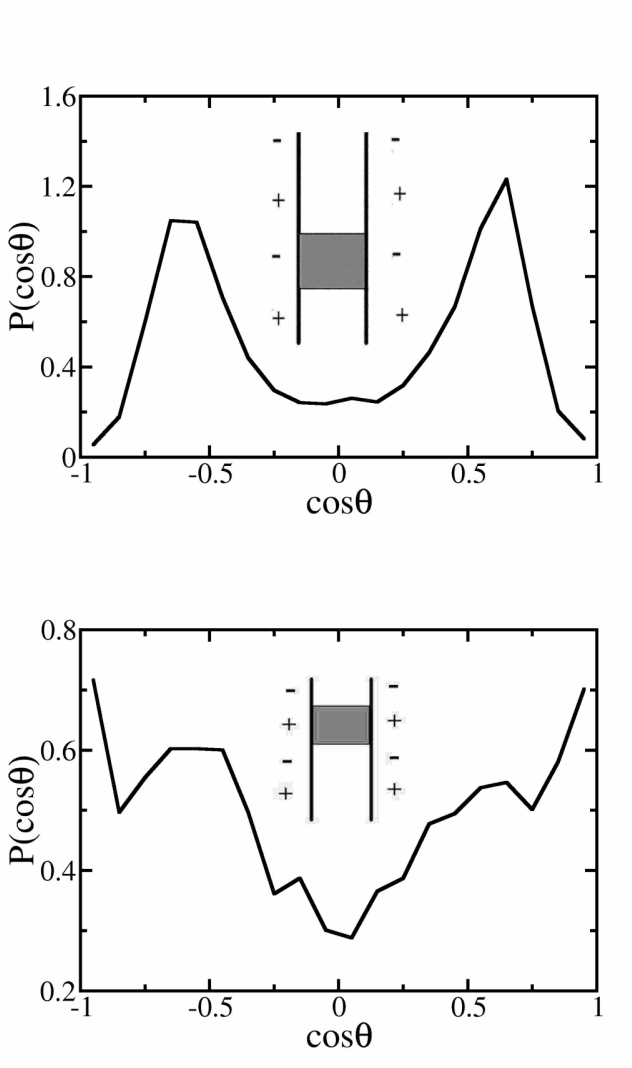

Figure 4.11: Water orientational distributions as in Figure 4.10, except that only appropriate portion (around one fourth of water molecules between two plates) was taken into account. Those water molecules are between (a) two negative charged portions of the plates and (b) two positively charged portions, as shown in the figures.

plates are shown in Figure 4.12. This time the two kinds of regions (positive–negative and negative–positive) are similar to each other, unlike it was for the type A system. Therefore we should expect that one dominant orientation and its mirror image prevail. From the plots of the orientational distributions, we conclude that almost all water molecules follow a type of orientation where one OH bond is pointing along the z axis and another OH bond is making an angle of 109.4^{o} with respect to the z axis. Due to the presence of two mirror images for water orientations there are two peaks in P_{OH} at ±1 and a broad peak around 0. The two peaks in the P_{μ} plot have the same origin, they emanate from the two kinds of space regions (positive–negative and negative–positive). By having this kind of orientation, a water molecule can form two close contacts with two opposite plate charges (water oxygen with the positive charge on the plate and water hydrogen with the negative plate charge). We can also see from the snapshot in Figure 4.12 that the number of water–water hydrogen contacts is decreased compared with that found for the A type systems and that the water hydrogen bonding network is less affected. In the case of two layers of water, as shown in Figure 4.13, the orientational distributions are similar to those found for the one layer case, except that the peaks are broader. This means that water molecules in every layer have similar orientations and that orientations in every layer are similar to the one found for water when only one layer is present between the plates. As in the one layer situation (system B), the two peaks in P_{μ} are due to the existence of two kinds of space regions (positive–negative and negative–positive). This can be seen from Figure 14 where we observe just one peak if we look at a negative–positive region. From the snapshot we can observe that the interactions between two water layers are not as unfavourable as those in the type A system, because the two layers of water molecules have the same orientation. This orientation arrangement is also

favourable for the formation of hydrogen bonds. Also, in this case we observe that many water-plate favourable contacts are formed.

In summary, water molecules in type B systems display orientational distributions that are quite different when compared to those in type A systems. When one layer of water is found between plates in the type B system, we observe that both water–plate and water–water interactions are more favourable. In the case of two layers of water, the water–plate interaction in type B systems may be as favourable as that in type A systems. But inter-layer water–water interactions in type B systems are much more favourable. Thus, we conclude, that at any distance the hydrogen bonding network in type B systems is less perturbed. Furthermore, when plates come closer, there are more energetically unfavourable water–water and water–plate contacts in the type A system compared to the type B system.

Hydrogen bonding analysis

In order to confirm the conclusion we reached above about the water–water hydrogen bonding network in different cases, we calculated the average number of hydrogen bonds per water molecule in each case. We used standard geometry criteria [9, 34] to calculate the number of hydrogen bonds. Two water molecules are considered to form a hydrogen bond if the inter-oxygen distance is less than 3.5Å and the O–H hydrogen bond distance is less than 2.45 Å and the H–O–O angle is less than 30^{o} . The same interpolate distances were used for calculations with one and two layers of water as used for the calculations of the plots in the previously presented figures. All the results were obtained from 500 ps trajectories. The data on the number of hydrogen bonds per water molecule are given in Table 4.1. These data are consistent with our previous discussion on the orientational distributions. In both A and B

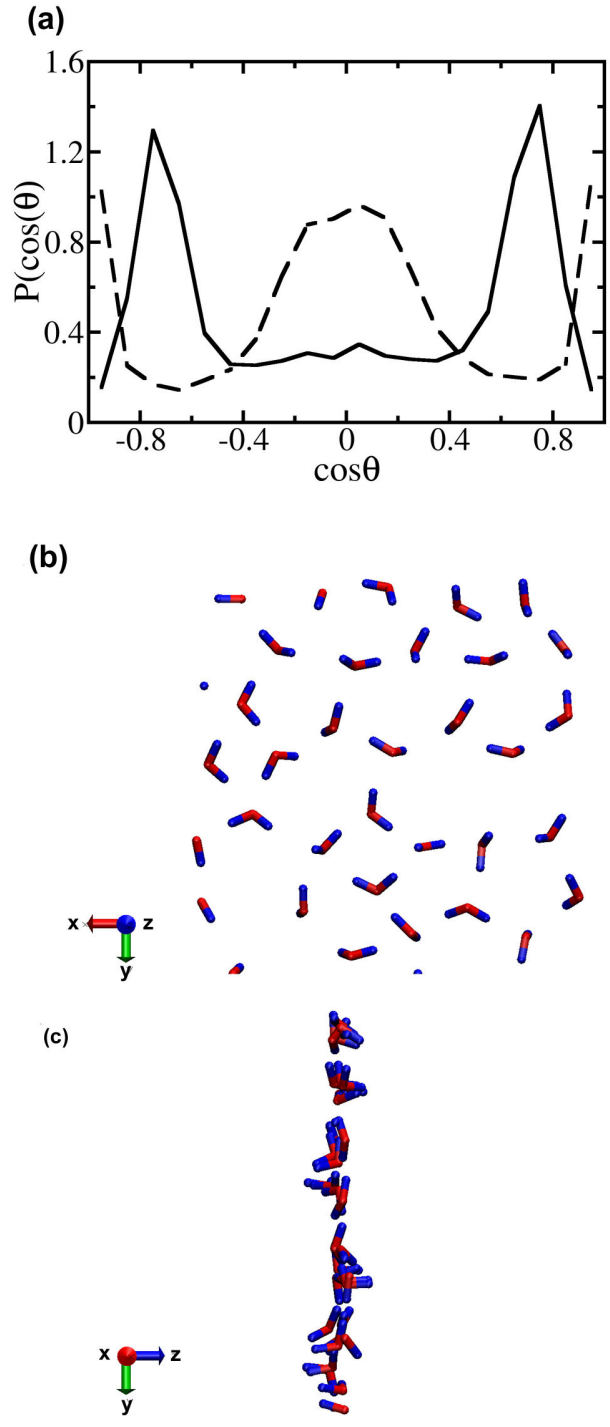

Figure 4.12: (a) Water orientational distributions in the type B system with r = 6.0Å. The meanings of θ and P(cosθ) are discussed in the text. The solid line is for $P_{\mu}(\cos\theta)$ and the dashed line is for $P_{OH}(\cos\theta)$. (b) The snapshot of water molecules; view from the xy plane. (c) The snapshot of water molecules; view from the yz plane.

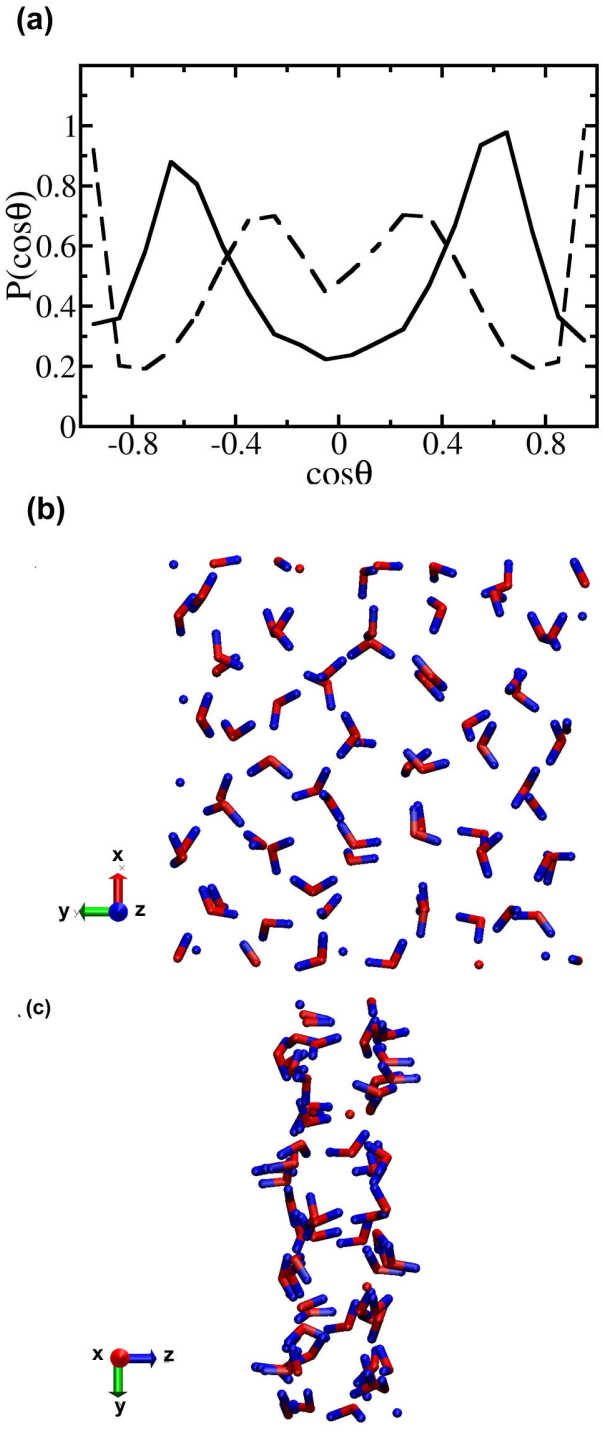

Figure 4.13: (a) Water orientational distributions in the type B system with r = 9.6Å. The meanings of θ and P(cosθ) are discussed in the text. The solid line is for $P_{\mu}(\cos\theta)$ and the dashed line is for $P_{OH}(\cos\theta)$. (b) The snapshot of water molecules; view from the xy plane. (c) The snapshot of water molecules; view from the yz plane.

Table 4.1: The average number of hydrogen bonds per water molecule for water between two plates in different situations.

	Non-charged	Type A	Type B
One layer of water	3.00	2.15	2.49
Two layers of water	3.26	3.03	3.15

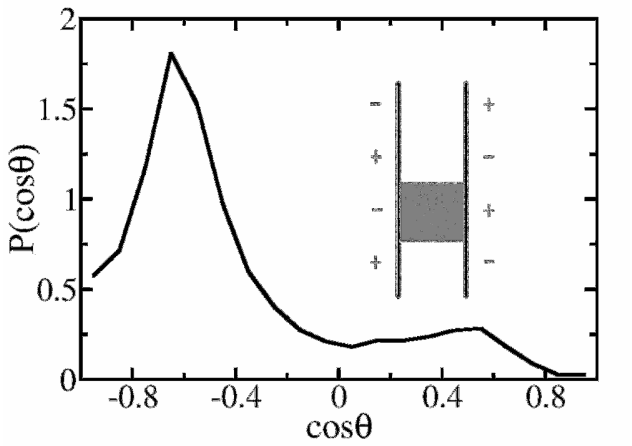

Figure 4.14: The orientational distribution $P_{\mu}(\cos\theta)$ for approximately one fourth of water molecules that are located between two portions of the plates, as shown in the figure.

type of systems, the artificial charges on the plates perturbed the water hydrogen bond network. But as we discussed before, in B type systems the number of hydrogen bonds per water molecule is larger compared with that found in type A systems.

4.4 Conclusions

We calculated the potential of the mean force acting between two model hydrophilic plates immersed in water. The model plates were represented by grapheme layers; the plates were electrically neutral but alternating rows of charges were placed on them to mimic the dipolar character of the phospholipid surfaces. Also, a different inter-plate charge correlation was studied. We have shown that the water contribution to the free-energy change can be either attractive or repulsive depending on the nature of the inter-plate direct interaction. In the current work we also demonstrate the possibility of solvent domination by reducing the correlation between plate charges and therefore the direct Coulomb interaction.

The potential of the mean force we obtained from our calculations was compared to the one that can be obtained by using the dielectric continuum description of solvent water. We observed that the continuum model predicts quite well the solvent effect for distances beyond 10Å when more than two layers of water separate the plates. For distances below 10Å the effect of water structure is very strong, and the free energy does not agree with the continuum description. We observed that the water contribution into the free-energy curves displays oscillations due to the molecular size of the water. From water orientational distributions and hydrogen bonding analysis we found that the hydrogen bond network in water between plates was disturbed by plate charges in both A and B cases and that the disturbance was stronger in the A case. The decrease in the number of hydrogen bonds per water molecule when water is embedded between surfaces produces a tendency for water to leave this space. It is the favourable water–surface interaction that may counterbalance the

water escaping tendency. In case A, when the hydrogen bonding network of water is strongly disturbed, the counterbalancing effect of the surface is not strong enough and water will try to leave the space between the plates. As a result, the water contribution into the PMF is attractive. In case B the hydrogen bonding disruption is smaller and the effect of surface charges is stronger. Thus, in this case water will attempt to enter the space between surfaces and its contribution to the PMF will be repulsive.

Although we considered here model systems we hope that they reproduce the basic physical nature of many models used to describe the hydration force between neutral membranes and our simulation results may be helpful in understanding such models and the experimental findings.

Chapter 5

Interactions of Cholesterol with DPPC and PSM Bilayers Studied by Molecular Dynamics Simulations

5.1 Introduction

The lipid-cholesterol interaction is of particular interest because of recent intensive research works on domains and rafts in lipid membranes [8] which are considered to be related to many biological membrane functions. The simplest raft formation in one model membrane involves three components including two kinds of lipids and cholesterol. In such a system, there are domains in the liquid-ordered phase with one kind of lipid as the main

component and a high cholesterol concentration. These rafts can coexist with another fluid (liquid-disordered) region mainly made of the second type of lipid and a low cholesterol concentration. One popular and the most straightforward idea of raft formation is that the two lipids have different interaction free energy with cholesterol [82]. In this case, the phase separation is driven by this free energy difference and the cholesterol rich rafts are formed due to better cholesterol affinity of one lipid. There are other opinions which believe the underground mechanism is more related to dynamics [59].Many experimental works have been performed in order to understand the lipid-cholesterol interaction for different lipids. Among various lipids, two phosphatidylcholine lipids DPPC/DOPC and sphingomyelin (SM) are often chosen as comparison purpose. This is because these lipids are used in many rafts formation experiments and the structure differences between them involve two major factors when discussing structure-affinity relationships. The two factors are the SM linkage and the lipid tail double bond. The general belief is that the lipid-cholesterol affinity follows the rule SM > saturated PC > unsaturated PC [82]. There are some experimental results [81, 82] clearly showing the stronger cholesterol affinity for saturated PC compared to that for unsaturated counterpart. But for the comparison between SM and saturated PC, contradictions exist in literature. There are a number of reports [30, 42] indicating that there is no special affinity between SM and cholesterol, while some other reports claim that this stronger affinity does exist [58, 82, 88].

Above confusion on SM-cholesterol affinity is related to the view on relative importance of the two lipid structure factors (the linkage and the tail), which is also unclear in the literature. The model membranes with SM and unsaturated lipids have been studied quite often because of their importance in raft forming experiments. There are some

theoretical models which explain the raft formation only based on the tail properties [21, 39]. On the other hand, the relationship between the lipid-cholesterol interaction and the SM-cholesterol hydrogen bonding property was studied in many molecular dynamics (MD) simulations [37, 62]. How much the two factors affect the lipid-cholesterol interaction is still an open question.

MD simulations with free energy calculations can be used to obtain the free energy change for removing one molecule out of a bilayer. In this way the affinity between the removed molecule and the bilayer can be studied. Here we present our free energy calculation works in order to provide some quantitative results which may help to answer the question that whether there is a special affinity due to the sphingomyelin linkage structure.

5.2 Simulation Details

We performed molecular dynamics (MD) simulations to obtain the potential of mean force (PMF) for removing one cholesterol molecule from lipid bilayers. In this way, we can obtain the free energy difference between states in which the cholesterol molecules are in the bilayer or in water solvent. In order to study the relationship between lipid molecular structure and cholesterol affinity, we simulated two different lipid bilayers in our molecular dynamics simulations. These bilayers were made of DPPC (di(16:0) PC), and N-palmitoyl-sphingomyelin (PSM) molecules. The numbers of lipid tail carbon atoms are the same for the two bilayer-forming lipids. Thus the lipids in the two systems have roughly the

same tail length. According to Lange et al., [42] the cholesterol affinity strongly depends on the length of the lipid tail. By comparing the two systems we can find the free energy difference only related to the SM linkage.

Each of the two systems in our simulations contained a bilayer of 70 DPPC/PSM and two cholesterol molecules. The bilayer was made from two leaflets that contain 35 DPPC/PSM and one cholesterol molecule respectively. The force field of the DPPC [5]/PSM [62] and cholesterol [31] molecules can be found in the literature. The whole bilayer was then solvated in 2465 SPC/E [3] water molecules. A 30ns MD simulation was performed for each of the systems, including 10ns for equilibrium and 20ns for collecting data. Bilayer properties, such as density profile were obtained using these simulation trajectories. Larger systems containing 3237 water molecules were also simulated with the same procedure. The final equilibrated configurations of above MD simulations were used as the initial conformations in our PMF calculations.

The umbrella sampling method with WHAM [41, 72] was used to calculate the PMF of removing one cholesterol molecule from the bilayer. There were 20 separate simulations (windows) with umbrella potential for each of the two systems. The umbrella potential was a simple harmonic potential added to the total Hamiltonian:

$$U_{umb} = k_{umb}(h - h_0)^2 \qquad (5.1)$$

with k_{umb} value 500.0 kJ/mol/nm^2. Here h is defined as the center of mass distance between the lipid bilayer and the cholesterol. One such window contained 10ns for equilibrium plus 20ns for collecting data. The PMFs were calculated as a function of the bilayer-cholesterol distance h. Because there was a cholesterol in the each of the two leaflets of the bilayer, each cholesterol was pulled out with the same distance h in opposite directions in each window.

By choosing various values of h_0 in each window, we obtained the probability distribution of cholesterol position. Finally, we obtained two PMFs for these two cholesterol molecules and for each of the two systems using WHAM formulas. In our simulations, the range of h_0 was from 0 to 3.8 nm with the Δh_0 value 0.2 nm between two neighboring windows. When h_0 was from 0 to 2.6 nm, the initial conformations were from the previous equilibrated systems with 2465 water molecules. The equilibrated configurations with 3237 water molecules were used as starting points for 2.8 to 3.8 nm h_0 range since a thicker water slab was needed in these cases to eliminate the periodic boundary effect.

The system temperature and pressure for all simulations were 319K and 1.01 bar in order to compare with the experimental results of Lange et al [42]. Corresponding correlation time τ_T and τ_P were 0.5 and 2.0 ps respectively for Nose-Hoover thermostat[63] and the Parrinello-Rahman barostat[64, 65]. In all simulations, the bond lengths were kept constant by applying LINCS algorithm [28]. PME method [22] was applied for long range coulomb forces. We performed our simulations with Gromacs package [4, 47].

5.3 Results and Discussions

The density profiles for various components have been shown in Figure 5.1 and Figure 5.2 for DPPC and PSM systems respectively. In both bilayer systems, the lipid densities decayed to zero at h value around ± 2.75 nm. In our umbrella sampling windows, the largest h_0 is 3.8 nm. In our simulations, the radius of one cholesterol molecule is around 0.64 nm estimated from radius of gyration data. Thus the largest value of h_0 was enough to keep the cholesterol molecules out of the bilayers. This can be confirmed by direct observations of MD trajectories as that shown in Figure 5.3.

The maximal density of cholesterol occurs at approximately ± 1 nm for both DPPC and PSM cases. These distances should be close to the PMF minima calculated from umbrella sampling method. The density profiles of cholesterol were not very smooth compared with that of lipids. This is due to there being one cholesterol molecule in each bilayer leaflet. Hence, the statistics for the cholesterol densities was quite poor. According to MacCallum and Tieleman [52], the positions of small molecules in the bilayer are highly dependent on the initial comditions of the simulation. In order to obtain the obtain the distribution density with better statistics, various free energy calculation methods are needed, such as the umbrella sampling method that used in this work.

The PMF curves for the two systems have been shown in Figure 5.4 and Figure 5.5. The features of the curves were similar to the PMF obtaining by Kim et al[38]., in which they calculated the PMF for removing liquid crystal-forming molecules from a DPPC bilayer. In each of the two PMF curves, there was a free energy minimum for small h, indicating the equilibrated location of the cholesterol molecule within the bilayer. This free energy

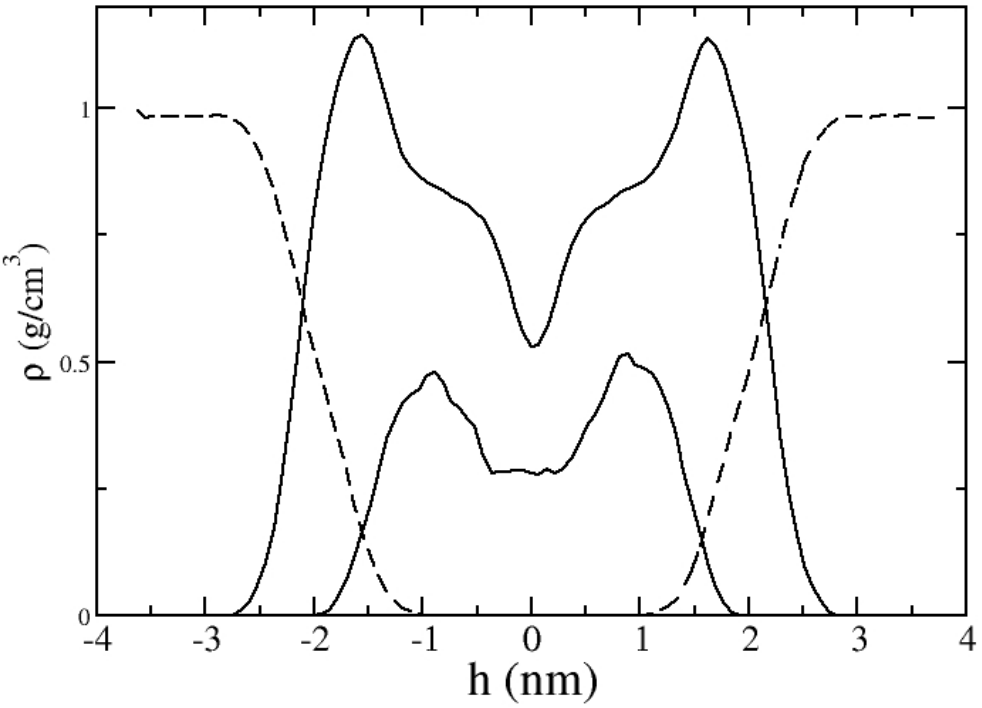

Figure 5.1: The density profiles for various components in our MD simulations for DPPC systems. The higher solid line is the density of DPPC. The lower solid line is the density of cholesterol molecules, which has been multiplied by 20 for clarity. The dashed line is the density of water.

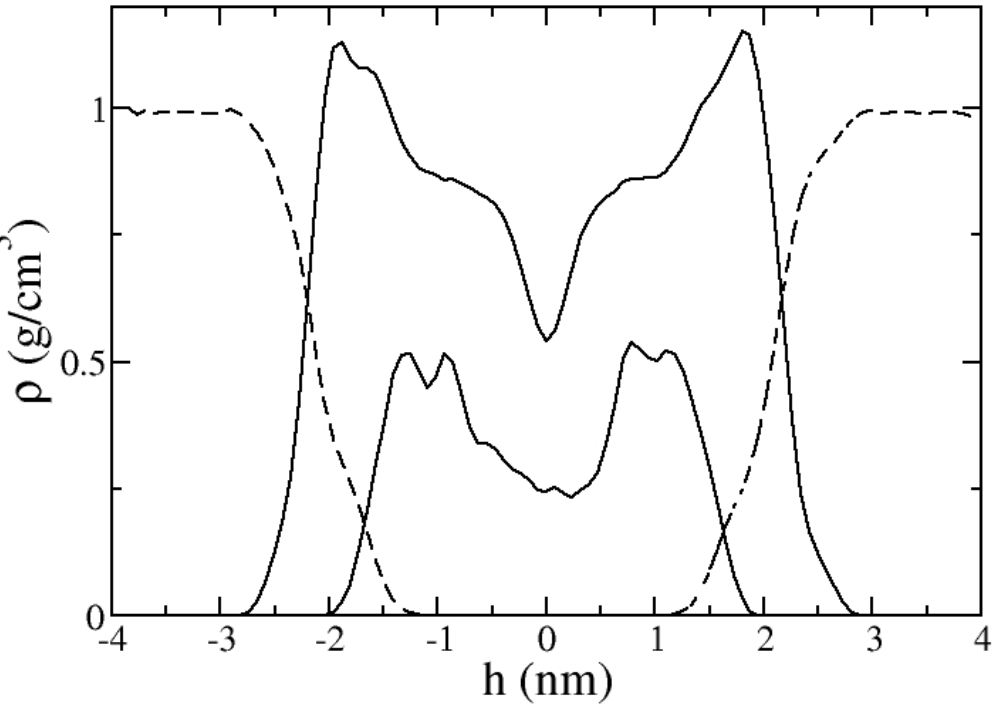

Figure 5.2: The density profiles for various components in our MD simulations for PMS systems. The higher solid line is the density of PSM. The lower solid line is the density of cholesterol molecules, which has been multiplied by 20 for clarity. The dashed line is the density of water.

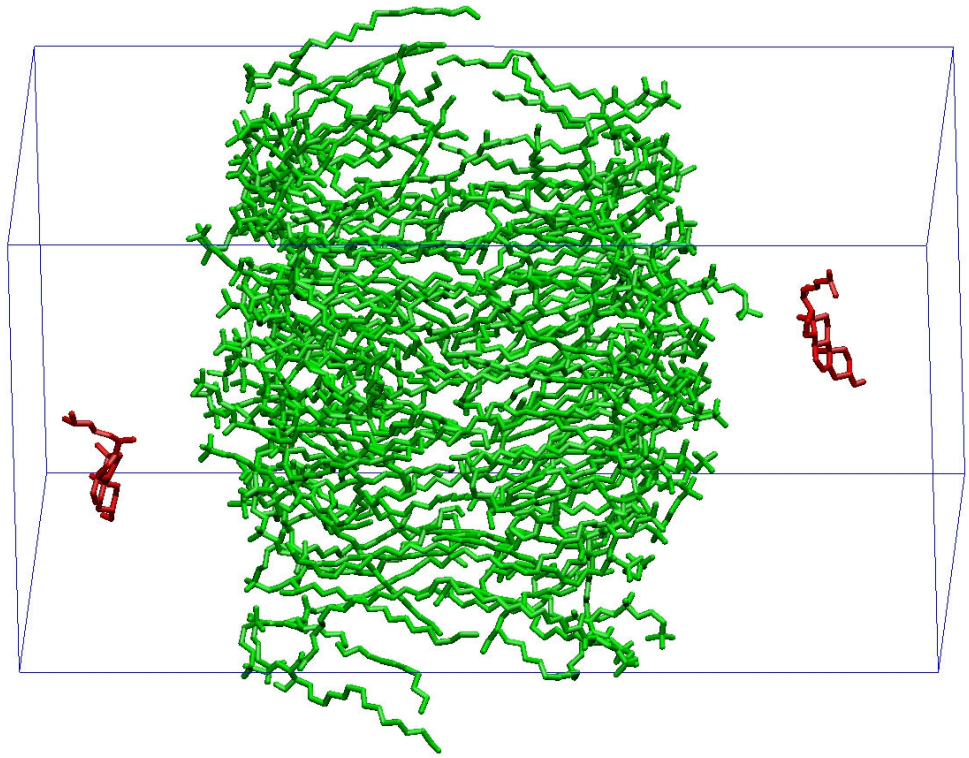

Figure 5.3: The snapshot of one window in PSM umbrella simulations for h_0=3.6 nm and t=30 ns. Red molecules are cholesterol molecules and green molecules are PSM molecules. Water were removed for clarity.

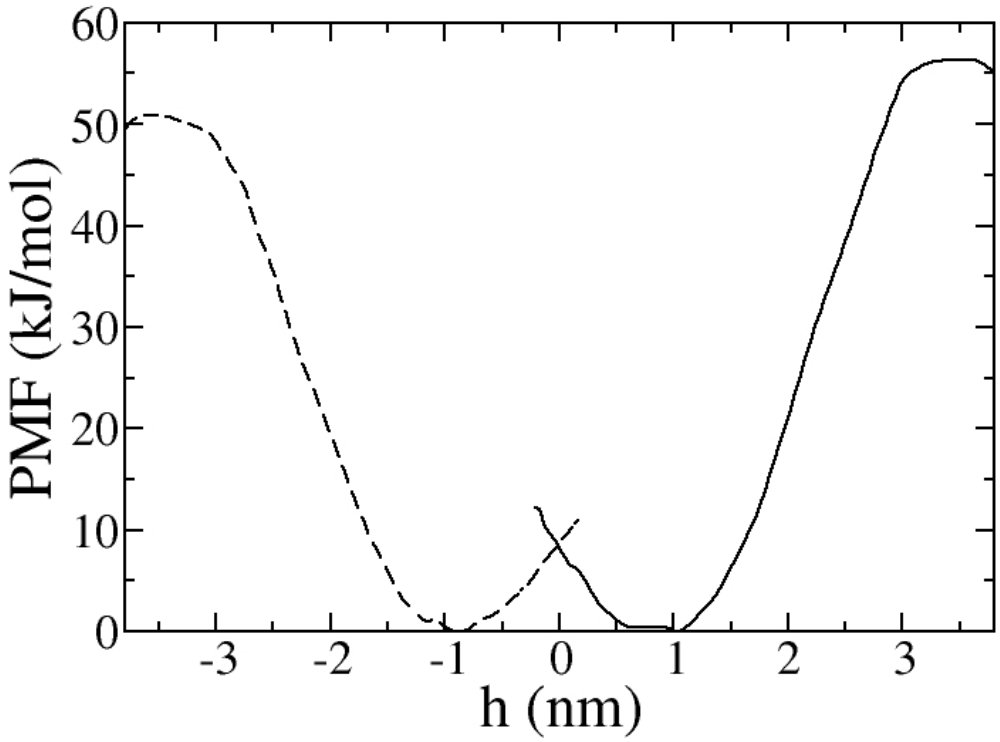

Figure 5.4: The PMF result for the DPPC case. The solid line is for the right leaflet and the dashed line is for the left leaflet.

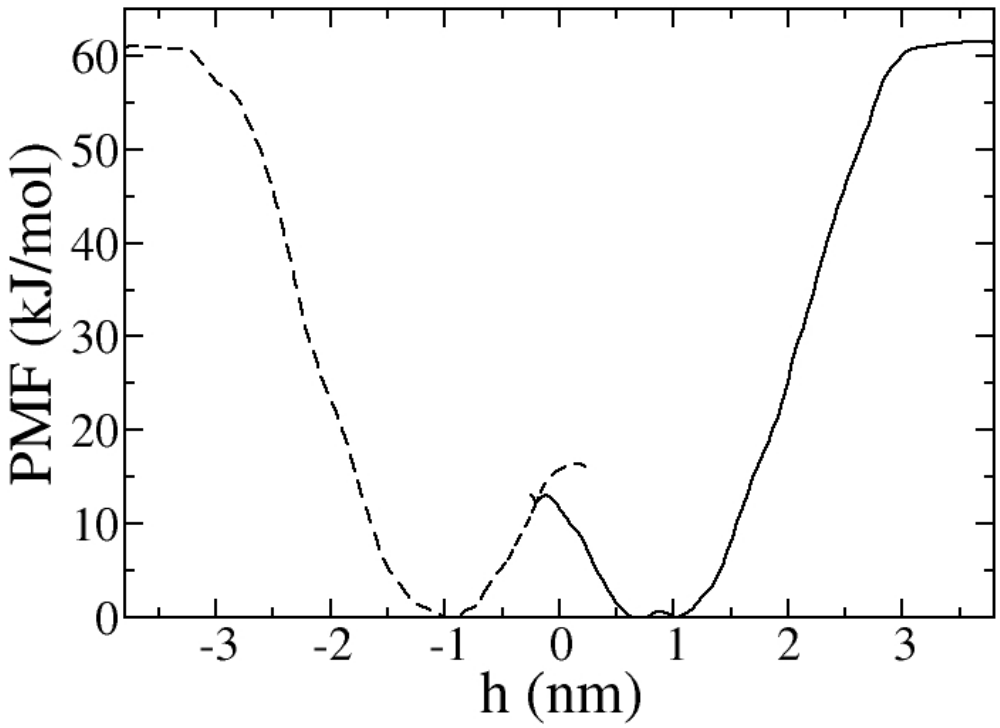

Figure 5.5: The PMF result for the PSM case. The solid line is for the right leaflet and the dashed line is for the left leaflet.

minimum occurred around ±1 nm for both of two systems and the results were consistent with density profiles. There was a free energy barrier while increasing h beyond the minimum point. It corresponded to the free energy penalty for removing the cholesterol molecule. After the cholesterol molecule was completed pulled out into the water solvent by further increasing h, the PMF curves became flat in this h region. There are small differences between our PMF curves and the curves from Kim et al[38]., especially in the two ends. These differences are considered to be the results of cholesterol interaction between the two leaflets. Unlike the work done by Kim et al[38]., in which they only had one cholesterol molecule in the bilayer, we put two cholesterol molecules symmetrically into the two bilayer leaflets. This was to effectively double the simulation length in order to obtain better statistics in free energy calculations. Another advantage of our system set up was to avoid any artificial effect due to the asymmetrical nature of the simulated system, such as that in the Ewald calculations[92]. Considering the computational time for all the MD simulations that we need to perform, we simulated very small systems. Thus the cholesterol-cholesterol interaction can not be neglected when h is very small and when h is large (due to the periodic boundary condition). This explains the curve shape we obtained in the two ends of the PMF curves that were slightly different from results in literature. But the most important information we need from the PMF curves is the free energy cost for removing the cholesterol molecule from the bilayer, which is directly related to cholesterol-bilayer affinity. We can therefore neglect the tails of the curves at the ends and define the free energy cost for pulling out one cholesterol molecule from the bilayer as $\Delta G_{pull} = G_{max} - G_{min}$, where G_{max} and G_{min} are the maximum and minimum values on each PMF curve.

The results of ΔG_{pull} are shown in Table 5.1. We notice that there is a large deviation

between ΔG_{pull} values that were calculated from the two leaflets of the same system. This indicates that the systems are easily trapped in meta-stable configurations and simulations with very long times are needed to obtain good average for this free energy difference. In principle, the ΔG_{pull} should only depend on the initial and final states rather than the pulling out process. Even though our simulation time was typical for similar bilayer simulations, the larger deviation in our results means that the system may be very likely trapped in some meta-stable conformations. We will only discuss our free energy results based on the average of the two leaflets. The similar asymmetric results can be also found in the work of MacCallum and Tieleman[52].

From the average values of ΔG_{pull} in Table 5.1, we found the free energy costs for removing one cholesterol obey the order PSM > DPPC. This result is consistent with the many cholesterol affinity experimental results mentioned in the introduction. That is, SM > saturated PC > unsaturated PC for cholesterol affinity. The free energy difference between the DPPC system and the PSM system is 7.6 kJ/mol. In the experimental work of Veatch et al[89]., the free energy difference for transferring cholesterol from a DPPC vesicle to a DOPC vesicle was estimated based on the equilibrium compositions of vesicles. Their result for 30ºC is 1.5-3 kJ/mol, which is in the same order of magnitude of our simulation result. A recent report from Tsamaloukas et al[86]. using calorimetry suggested the same order of magnitude cholesterol affinity difference between SM and POPC. As what we discussed above, the small magnitude of the free energy difference requires more simulation time or more advanced statistical methods in future simulation studies to obtain a more accurate quantitative comparison. Because tail carbon numbers are the same for both bilayer forming molecules in our simulations, the only effect having influence on ΔG_{pull} is the SM linkage.

Our results confirmed some experimental conclusions that the SM linkage can increase the cholesterol affinity. In many theoretical studies of lipid bilayers with cholesterol, the SM linkage is considered to be able to change the SM-cholesterol hydrogen bonding network[37, 62]. Thus a SM bilayer has a better cholesterol affinity than other lipid bilayers. From our data we conclude that the SM linkage plays an important role for the cholesterol affinity difference between SM and PC bilayers.

Table 5.1: The results of free energy cost ΔG_{pull} for pulling out a cholesterol molecule out of a bilayer. Units are in kJ/mol.

	Left leaflet	Right leaflet	average
DPPC system	50.92	56.37	53.64
PSM system	60.97	61.47	61.22

5.4 Conclusions

We performed MD simulations to calculate the free energy differences for removing one cholesterol molecule from various bilayers. We belive our results can help in understanding some contradictions on the cholesterol-bilayer affinity for a number of experimental results. From our simulation results, we found that there was indeed a stronger cholesterol affinity in the order of several kJ/mol for SM molecules compared with that for saturated DPPC. This increased cholesterol affinity is due to the SM linkage.

REFERENCES

Various Parts of this work, including excerpts of text, figures, and tables have been taken from the following references: [48-51] with appropriate permissions obtained from the American Institute of Physics, American Chemical Society, and Taylor & Francis.

[1] *Discover User Guide Part I*. Biosym Technologies, CA: 1993.

[2] P. Attard, and M. T. Batchelor. A Mechanism For The Hydration Force Demonstrated In A Model System. *Chem. Phys. Lett.* 149, (2), 206-211, 1988.

[3] H. J. C. Berendsen,J. R. Grigera, and T. P. Straatsma. The Missing Term In Effective Pair Potentials. *J. Phys. Chem.* 91, (24), 6269-6271, 1987.

[4] H. J. C. Berendsen,D. Vanderspoel, and R. Vandrunen. Gromacs - A Message-Passing Parallel Molecular-Dynamics Implementation. *Comput. Phys. Commun.* 91, (1-3), 43-56, 1995.

[5] O. Berger,O. Edholm, and F. Jahnig. Molecular dynamics simulations of a fluid bilayer of dipalmitoylphosphatidylcholine at full hydration, constant pressure, and constant temperature. *Biophys. J.* 72, (5), 2002-2013, 1997.

[6] M. L. Berkowitz, and K. Raghavan. Computer-Simulation Of A Water Membrane Interface. *Langmuir* 7, (6), 1042-1044, 1991.

[7] N. A. M. Besseling. Theory of hydration forces between surfaces. *Langmuir* 13, (7), 2113-2122, 1997.

[8] W. H. Binder,V. Barragan, and F. M. Menger. Domains and rafts in lipid membranes. *Angew. Chem.-Int. Edit.* 42, (47), 5802-5827, 2003.

[9] I. Chandrasekhar,C. Oostenbrink, and W. F. van Gunsteren. Simulating the physiological phase of hydrated DPPC bilayers: The ester moiety. *Soft Mater.* 2, (1), 27-45, 2004.

[10]N. Choudhury, and B. M. Pettitt. On the mechanism of hydrophobic association of nanoscopic solutes. *J. Am. Chem. Soc.* 127, (10), 3556-3567, 2005.

[11] W. D. Cornell,P. Cieplak,C. I. Bayly,I. R. Gould,K. M. Merz,D. M. Ferguson,D. C. Spellmeyer,T. Fox,J. W. Caldwell, and P. A. Kollman. A 2nd Generation Force-Field For The Simulation Of Proteins, Nucleic-Acids, And Organic-Molecules. *J. Am. Chem. Soc.* 117, (19), 5179-5197, 1995.

[12] S. R. P. da Rocha,K. P. Johnston, and P. J. Rossky. Surfactant-modified CO2-water interface: A molecular view. *J. Phys. Chem. B* 106, (51), 13250-13261, 2002.

[13] S. R. P. da Rocha,K. P. Johnston,R. E. Westacott, and P. J. Rossky. Molecular structure of the water-supercritical CO2 interface. *J. Phys. Chem. B* 105, (48), 12092-12104, 2001.

[14] S. K. Das,M. M. Sharma, and R. S. Schechter. Solvation force in confined molecular fluids using molecular dynamics simulation. *J. Phys. Chem.* 100, (17), 7122-7129, 1996.

[15] P. Dauber-Osguthorpe,V. A. Roberts,D. J. Osguthorpe,J. Wolff,M. Genest, and A. T. Hagler. Structure And Energetics Of Ligand-Binding To Proteins - Escherichia-Coli Dihydrofolate Reductase Trimethoprim, A Drug-Receptor System. *Proteins* 4, (1), 31-47, 1988.

[16] A. de Vries,S. J. Marrink, and A. Mark. Molecular dynamics simulations of spontaneous aggregation and millisecond dynamics of mixed cholesterol/DPPC bilayers. *Biophys. J.* 84, (2), 463A-463A, 2003.

[17] B. V. Derjaguin, and L. D. Landau. *Acta Physicochim. URSS* 14, 633, 1941.

[18] P. Diep,K. D. Jordan,J. K. Johnson, and E. J. Beekman. CO2-fluorocarbon and CO2-hydrocarbon interactions from first-principles calculations. *J. Phys. Chem. A* 102, (12), 2231-2236, 1998.

[19] H. Dominguez, and M. L. Berkowitz. Computer simulations of sodium dodecyl sulfate at liquid/liquid and liquid/vapor interfaces. *J. Phys. Chem. B* 104, (22), 5302-5308, 2000.

[20] J. Eastoe,A. Dupont, and D. C. Steytler. Fluorinated surfactants in supercritical CO2. *Curr. Opin. Colloid Interface Sci.* 8, (3), 267-273, 2003.

[21] R. Elliott,K. Katsov,M. Schick, and I. Szleifer. Phase separation of saturated and mono-unsaturated lipids as determined from a microscopic model. *J. Chem. Phys.* 122, (4), 2005.

[22] U. Essmann,L. Perera,M. L. Berkowitz,T. Darden,H. Lee, and L. G. Pedersen. A Smooth Particle Mesh Ewald Method. *J. Chem. Phys.* 103, (19), 8577-8593, 1995.

[23] J. Faraudo, and F. Bresme. Anomalous dielectric behavior of water in ionic Newton black films. *Phys. Rev. Lett.* 92, (23), 2004.

[24] J. Faraudo, and F. Bresme. Origin of the short-range, strong repulsive force between ionic surfactant layers. *Phys. Rev. Lett.* 94, (7), 2005.

[25] M. F. C. Gomes, and A. A. H. Padua. Interactions of carbon dioxide with liquid fluorocarbons. *J. Phys. Chem. B* 107, (50), 14020-14024, 2003.

[26] D. W. R. Gruen, and S. Marcelja. Spatially Varying Polarization In Water - A Model For The Electric Double-Layer And The Hydration Force. 79, 225-242, 1983.

[27] J. G. Harris, and K. H. Yung. Carbon Dioxides Liquid-Vapor Coexistence Curve And Critical Properties As Predicted By A Simple Molecular-Model. *J. Phys. Chem.* 99, (31), 12021-12024, 1995.

[28] B. Hess,H. Bekker,H. J. C. Berendsen, and J. Fraaije. LINCS: A linear constraint solver for molecular simulations. *J. Comput. Chem.* 18, (12), 1463-1472, 1997.

[29] H. Higashi,Y. Iwai,H. Uchida, and Y. Arai. Diffusion coefficients of aromatic compounds in supercritical carbon dioxide using molecular dynamics simulation. *J. Supercrit. Fluids* 13, (1-3), 93-97, 1998.

[30] J. M. Holopainen,A. J. Metso,J. P. Mattila,A. Jutila, and P. K. J. Kinnunen. Evidence for the lack of a specific interaction between cholesterol and sphingomyelin. *Biophys. J.* 86, (3), 1510-1520, 2004.

[31] M. Holtje,T. Forster,B. Brandt,T. Engels,W. von Rybinski, and H. D. Holtje. Molecular dynamics simulations of stratum corneum lipid models: fatty acids and cholesterol. *Biochim. Biophys. Acta-Biomembr.* 1511, (1), 156-167, 2001.

[32] W. G. Hoover. Canonical Dynamics - Equilibrium Phase-Space Distributions. *Phys. Rev. A* 31, (3), 1695-1697, 1985.

[33] J. N. Israelachvili, and H. Wennerstrom. Hydration Or Steric Forces Between

Amphiphilic Surfaces. 6, (4), 873-876, 1990.

[34] P. Jedlovszky,J. P. Brodholt,F. Bruni,M. A. Ricci,A. K. Soper, and R. Vallauri. Analysis of the hydrogen-bonded structure of water from ambient to supercritical conditions. *J. Chem. Phys.* 108, (20), 8528-8540, 1998.

[35] K. P. Johnston,K. L. Harrison,M. J. Clarke,S. M. Howdle,M. P. Heitz,F. V. Bright,C. Carlier, and T. W. Randolph. Water in carbon dioxide microemulsions: An environment for hydrophiles including proteins. *Science* 271, (5249), 624-626, 1996.

[36] W. L. Jorgensen, and J. Gao. Monte-Carlo Simulations Of The Hydration Of Ammonium And Carboxylate Ions. *J. Phys. Chem.* 90, (10), 2174-2182, 1986.

[37] G. A. Khelashvili, and H. L. Scott. Combined Monte Carlo and molecular dynamics simulation of hydrated 18: 0 sphingomyelin-cholesterol lipid bilayers. *J. Chem. Phys.* 120, (20), 9841-9847, 2004.

[38] E. B. Kim,N. Lockwood,M. Chopra,O. Guzman,N. L. Abbott, and J. J. de Pablo. Interactions of liquid crystal-forming molecules with phospholipid bilayers studied by molecular dynamics simulations. *Biophys. J.* 89, (5), 3141-3158, 2005.

[39] S. Komura,H. Shirotori,P. D. Olmsted, and D. Andelman. Lateral phase separation in mixtures of lipids and cholesterol. *Europhys. Lett.* 67, (2), 321-327, 2004.

[40] A. A. Kornyshev, and S. Leikin. Fluctuation Theory Of Hydration Forces - The Dramatic Effects Of Inhomogeneous Boundary-Conditions. *Phys. Rev. A* 40, (11), 6431-6437, 1989.

[41] S. Kumar,D. Bouzida,R. H. Swendsen,P. A. Kollman, and J. M. Rosenberg. The Weighted Histogram Analysis Method For Free-Energy Calculations On Biomolecules.1. The Method. *J. Comput. Chem.* 13, (8), 1011-1021, 1992.

[42] Y. Lange,J. S. Dalessandro, and D. M. Small. Affinity Of Cholesterol For Phosphatidylcholine And Sphingomyelin. 556, (3), 388-398, 1979.

[43] D. Leckband, and J. Israelachvili. Intermolecular forces in biology. *Q. Rev. Biophys.* 34, (2), 105-267, 2001.

[44] S. Leikin. On The Theory Of Electrostatic Interaction Of Neutral Lipid Bilayers

Separated By Thin Water Film. *J. Chem. Phys.* 95, (7), 5224-5229, 1991.

[45] S. Leikin,V. A. Parsegian,D. C. Rau, and R. P. Rand. Hydration Forces. *Annu. Rev. Phys. Chem.* 44, 369-395, 1993.

[46] D. M. Leneveu,R. P. Rand, and V. A. Parsegian. Measurement Of Forces Between Lecithin Bilayers. *Nature* 259, (5544), 601-603, 1976.

[47] E. Lindahl,B. Hess, and D. van der Spoel. GROMACS 3.0: a package for molecular simulation and trajectory analysis. *J. Mol. Model.* 7, (8), 306-317, 2001.

[48] L. Lu, and M. L. Berkowitz. Molecular dynamics simulation of a reverse micelle self assembly in supercritical CO2. *J. Am. Chem. Soc.* 126, (33), 10254-10255, 2004.

[49] L. Lu, and M. L. Berkowitz. Hydration force between model hydrophilic surfaces: Computer simulations. *J. Chem. Phys.* 124, (10), 2006.

[50] L. Lu, and M. L. Berkowitz. *Mol. Phys.*, 2007, accepted.

[51] L. Y. Lu, and M. L. Berkowitz. The effect of the rigidity of perfluoropolyether surfactant on its behavior at the water/supercritical carbon dioxide interface. *J. Phys. Chem. B* 109, (46), 21725-21731, 2005.

[52] J. L. MacCallum, and D. P. Tieleman. Computer simulation of the distribution of hexane in a lipid bilayer: Spatially resolved free energy, entropy, and enthalpy profiles. *J. Am. Chem. Soc.* 128, (1), 125-130, 2006.

[53] M. Manciu, and E. Ruckenstein. Oscillatory and monotonic polarization. The polarization contribution to the hydration force. *Langmuir* 17, (24), 7582-7592, 2001.

[54] M. Manciu, and E. Ruckenstein. Polarization of water near dipolar surfaces: A simple model for anomalous dielectric behavior. *Langmuir* 21, (25), 11749-11756, 2005.

[55] S. Marcelja, and N. Radic. Repulsion Of Interfaces Due To Boundary Water. *Chem. Phys. Lett.* 42, (1), 129-130, 1976.

[56] S. J. Marrink, and A. Mark. Molecular dynamics simulations of spontaneous formation and fusion of vesicles. *Biophys. J.* 84, (2), 135A-135A, 2003.

[57] S. J. Marrink,D. P. Tieleman, and A. E. Mark. Molecular dynamics simulation of the kinetics of spontaneous micelle formation. *J. Phys. Chem. B* 104, (51), 12165-12173, 2000.

[58] P. Mattjus, and J. P. Slotte. Does cholesterol discriminate between sphingomyelin and phosphatidylcholine in mixed monolayers containing both phospholipids? *Chem. Phys. Lipids* 81, (1), 69-80, 1996.

[59] S. Mayor, and M. Rao. Rafts: Scale-dependent, active lipid organization at the cell surface. *Traffic* 5, (4), 231-240, 2004.

[60] T. J. McIntosh, and S. A. Simon. Contributions Of Hydration And Steric (Entropic) Pressures To The Interactions Between Phosphatidylcholine Bilayers - Experiments With The Subgel Phase. 32, (32), 8374-8384, 1993.

[61] K. Nagashima,C. T. Lee,B. Xu,K. P. Johnston,J. M. DeSimone, and C. S. Johnson. NMR studies of water transport and proton exchange in water-in-carbon dioxide microemulsions. *J. Phys. Chem. B* 107, (9), 1962-1968, 2003.

[62] P. Niemela,M. T. Hyvonen, and I. Vattulainen. Structure and dynamics of sphingomyelin bilayer: Insight gained through systematic comparison to phosphatidylcholine. *Biophys. J.* 87, (5), 2976-2989, 2004.

[63] S. Nose. A Unified Formulation Of The Constant Temperature Molecular-Dynamics Methods. *J. Chem. Phys.* 81, (1), 511-519, 1984.

[64] S. Nose, and M. L. Klein. Constant Pressure Molecular-Dynamics For Molecular-Systems. *Mol. Phys.* 50, (5), 1055-1076, 1983.

[65] M. Parrinello, and A. Rahman. Polymorphic Transitions In Single-Crystals - A New Molecular-Dynamics Method. *J. Appl. Phys.* 52, (12), 7182-7190, 1981.

[66] R. M. Pashley, and J. N. Israelachvili. Molecular Layering Of Water In Thin-Films Between Mica Surfaces And Its Relation To Hydration Forces. *J. Colloid Interface Sci.* 101, (2), 511-523, 1984.

[67] L. Perera,U. Essmann, and M. L. Berkowitz. Role of water in the hydration force acting between lipid bilayers. *Langmuir* 12, (11), 2625-2629, 1996.

[68] A. Pertsin,D. Platonov, and M. Grunze. Direct computer simulation of water-mediated force between supported phospholipid membranes. *J. Chem. Phys.* 122, (24), 2005.

[69] R. Rajagopalan. Simulations of self-assembling systems. *Curr. Opin. Colloid Interface Sci.* 6, (4), 357-365, 2001.

[70] R. P. Rand,N. Fuller,V. A. Parsegian, and D. C. Rau. Variation In Hydration Forces Between Neutral Phospholipid-Bilayers - Evidence For Hydration Attraction. *Biochemistry* 27, (20), 7711-7722, 1988.

[71] D. C. Rau,B. Lee, and V. A. Parsegian. Measurement Of The Repulsive Force Between Poly-Electrolyte Molecules In Ionic Solution - Hydration Forces Between Parallel Dna Double Helices. 81, (9), 2621-2625, 1984.

[72] B. Roux. The Calculation Of The Potential Of Mean Force Using Computer-Simulations. *Comput. Phys. Commun.* 91, (1-3), 275-282, 1995.

[73] J. S. Rowlinson, and B. Widom, *Molecular Theory of Capillarity*. Clarendon press: Oxford, 1982.

[74] S. Salaniwal,S. T. Cui,H. D. Cochran, and P. T. Cummings. Molecular simulation of a dichain surfactant water carbon dioxide system. 2. Self-assembly and aggregation dynamics. *Langmuir* 17, (5), 1784-1792, 2001.

[75] S. Salaniwal,S. T. Cui,H. D. Cochran, and P. T. Cummings. Molecular simulation of a dichain surfactant water carbon dioxide system. 1. Structural properties of aggregates. *Langmuir* 17, (5), 1773-1783, 2001.

[76] D. Schiby, and E. Ruckenstein. The Role Of The Polarization Layers In Hydration Forces. *Chem. Phys. Lett.* 95, (4-5), 435-438, 1983.

[77] J. Schlitter. Estimation Of Absolute And Relative Entropies Of Macromolecules Using The Covariance-Matrix. *Chem. Phys. Lett.* 215, (6), 617-621, 1993.

[78] S. Senapati, and M. L. Berkowitz. Molecular dynamics simulation studies of polyether and perfluoropolyether surfactant based reverse micelles in supercritical carbon dioxide. *J. Phys. Chem. B* 107, (47), 12906-12916, 2003.

[79] S. Senapati,J. S. Keiper,J. M. DeSimone,G. D. Wignall,Y. B. Melnichenko,H. Frielinghaus, and M. L. Berkowitz. Structure of phosphate fluorosurfactant based reverse micelles in supercritical carbon dioxide. *Langmuir* 18, (20), 7371-7376, 2002.

[80] E. M. Sevick,P. A. Monson, and J. M. Ottino. Monte-Carlo Calculations Of Cluster Statistics In Continuum Models Of Composite Morphology. *J. Chem. Phys.* 88, (2), 1198-1206, 1988.

[81] S. R. Shaikh,V. Cherezov,M. Caffrey,S. P. Soni,D. LoCascio,W. Stillwell, and S. R. Wassall. Molecular organization of cholesterol in unsaturated phosphatidylethanolamines: X-ray diffraction and solid state H-2 NMR reveal differences with phosphatidylcholines. *J. Am. Chem. Soc.* 128, (16), 5375-5383, 2006.

[82] J. R. Silvius. Role of cholesterol in lipid raft formation: lessons from lipid model systems. *Biochim. Biophys. Acta-Biomembr.* 1610, (2), 174-183, 2003.

[83] M. T. Stone,P. G. Smith,S. R. P. da Rocha,P. J. Rossky, and K. P. Johnston. Low interfacial free volume of stubby surfactants stabilizes water-in-carbon dioxide microemulsions. *J. Phys. Chem. B* 108, (6), 1962-1966, 2004.

[84] I. Szleifer,A. Ben-shaul, and W. M. Gelbart. Chain Packing Statistics And Thermodynamics Of Amphiphile Monolayers. *J. Phys. Chem.* 94, (12), 5081-5089, 1990.

[85] A. Trokhymchuk,D. Henderson, and D. T. Wasan. A molecular theory of the hydration force in an electrolyte solution. *J. Colloid Interface Sci.* 210, (2), 320-331, 1999.

[86] A. Tsamaloukas,H. Szadkowska, and H. Heerklotz. Thermodynamic comparison of the interactions of cholesterol with unsaturated phospholipid and sphingomyelins. *Biophys. J.* 90, (12), 4479-4487, 2006.

[87] J. J. Valle-Delgado,J. A. Molina-Bolivar,F. Galisteo-Gonzalez,M. J. Galvez-Ruiz,A. Feiler, and M. W. Rutland. Hydration forces between silica surfaces: Experimental data and predictions from different theories. *J. Chem. Phys.* 123, (3), 2005.

[88] B. Y. van Duyl,D. Ganchev,V. Chupin,B. de Kruijff, and J. A. Killian. Sphingomyelin is much more effective than saturated phosphatidylcholine in excluding unsaturated phosphatidylcholine from domains formed with cholesterol. *FEBS Lett.* 547, (1-3), 101-106, 2003.

[89] S. L. Veatch,I. V. Polozov,K. Gawrisch, and S. L. Keller. Liquid domains in vesicles investigated by NMR and fluorescence microscopy. *Biophys. J.* 86, (5), 2910-2922, 2004.

[90] E. J. W. Verwey, and J. T. G. Overbeek, *Theory of Stability of Colloids*. Elsevier, Amsterdam: 1948.

[91] I. C. Yeh, and M. L. Berkowitz. Dielectric constant of water at high electric fields: Molecular dynamics study. *J. Chem. Phys.* 110, (16), 7935-7942, 1999.

[92] I. C. Yeh, and M. L. Berkowitz. Ewald summation for systems with slab geometry. *J. Chem. Phys.* 111, (7), 3155-3162, 1999.

[93] C. R. Yonker, and B. J. Palmer. Investigation of CO2/fluorine interactions through the intermolecular effects on the H-1 and F-19 shielding of CH3F and CHF3 at various temperatures and pressures. *J. Phys. Chem. A* 105, (2), 308-314, 2001.

[94] J. Zheng,L. Y. Li,H. K. Tsao,Y. J. Sheng,S. F. Chen, and S. Y. Jiang. Strong repulsive forces between protein and oligo (ethylene glycol) self-assembled monolayers: A molecular simulation study. *Biophys. J.* 89, (1), 158-166, 2005.

[95] R. G. Zielinski,S. R. Kline,E. W. Kaler, and N. Rosov. A small-angle neutron scattering study of water in carbon dioxide microemulsions. *Langmuir* 13, (15), 3934-3937, 1997.